

AMT-2016-366: Responses to Anonymous Reviewer

1

Stephen Broccardo

June 20, 2017

Thank you for your positive review and comments.

The title of the paper has been changed to reflect the fact that the results are specifically from the Highveld.

In response to the specific comments:

Page 2, Line 32: The slant density is the integral of the path length times the number density of that absorber, not the concentration (which describes the number density absorber as a fraction of the total air density).

Response and action

Agreed. Edited p2. line 32 and p3. line 4: changed the word “concentration” to “molecular number density”.

Page 3, Line 4: “to a first approximation, is slanted” is a bit confusing. Do you mean because of geometry?

Response and action

Yes, a geometric first approximation is what is meant. Added the word “geometric” to the sentence.

Page 3, Line 12: The analysis of the NO₂ slant column is skimmed over without really any detail. I realize there is another paper describing this process, but could you say a few words about what other absorbers and parameters are fit, as well as individual fitting uncertainties from noise or systematic uncertainties? Also, not much info on instrument. What is SNR, are these from spectra that have been co-added spatially, what is the size of the CCD array (pixels), spectral resolution, spectral sampling etc? What is used for a reference spectrum?

Page 4, Line 2: Can you expand just briefly on why a photolytic converter is desirable? Also, why do you present NO_y and not NO₂?

Response and Action

In response to these two questions, the description of the measurements has been expanded. The paragraphs now read:

A DOAS instrument based on an Acton 300i imaging spectrograph employing a pushbroom viewing geometry, where each line of pixels across the instrument's swath is captured simultaneously on an Andor DU-420BU CCD, was fitted into the Aerocommander 690A. This CCD has 255 pixels in the across-track dimension and 1024 pixels in the spectral direction. The temperature of the spectrograph was kept stable at 30°C using a thermostatic heater in an insulated box, and the CCD temperature was set at -20°C using its own in-built thermo-electric cooler. Eight spectra were co-added into 32 across-track pixels, each with an across-track footprint of approximately 70m, assuming a flight altitude of 4500m above the ground. This was done in order to make optimum use of the optical resolution of the instrument. Along-track resolution is determined by the aircraft speed and the integration time on the instrument, which was adjusted automatically in-flight to avoid saturation of the CCD, and is generally about 100m (Heue et al, 2008). In the present study only the nadir pixel of the iDOAS is used.

Slant-column densities were retrieved using the WinDOAS software package. Absorption cross-sections for NO₂ (Vandaele et al, 1998), ozone (Burrows et al, 1999), water vapour (Rothman et al, 1998), O₄ (Greenblatt et al, 1990) were fitted across a spectral range of 432nm to 464nm. The Ring effect was accounted for using a appropriate cross-section calculated using the DOASIS software (Kraus, 2006). A reference spectrum was chosen from an appropriate location along the flight track far from known sources implying that slant-column densities from WinDOAS are in fact differential slant column densities. Satellite retrievals use a similar technique, using a measurement over remote ocean areas as an approximation of zero-NO₂. We adjust our slant-column densities using an offset in order to bring the vertical column densities from the iDOAS into line with the appropriate satellite measurement (either OMI or SCIAMACHY) in background areas of our flight track.

In addition to the imaging DOAS (iDOAS) instrument, the aircraft carried a Particle Measurement Systems Passive Cavity Aerosol Spectrometer Probe 100X (PCASP), operated with the pre-heater switched on; and a Thermo Scientific 42i chemiluminescence instrument with a molybdenum converter in the cabin, plumbed into the aircraft's scientific-air inlet in order to measure in-situ NO_y. In such instruments the converter converts NO₂ to NO, which is then measured by chemiluminescence; however a molybdenum converter also converts other nitrogen species. This can be avoided using a photolytic converter, however an instrument with a photolytic converter to measure NO₂ was not within the project's budget. The aircraft is fitted with a Rosemount ambient temperature sensor, and a separate pitot-static

system for measurement and logging of static and dynamic pressure. The humidity sensor fitted to the aircraft did not function during this campaign. The aircraft's data acquisition system also logged parameters from a GPS (Global Positioning System) receiver.

Section 2: *Subheadings would increase the readability of this section. For example: “iDOAS NO₂”, “In situ measurements”, “Satellite observations” etc.*

Response and action

Subheadings have been added, and some of the paragraphs re-arranged to be under the relevant heading.

Page 4, Line 16: *This only the best case at nadir. The sides of the OMI swath are much larger.*

Response and action

The broadening of the OMI ground-pixel size towards the edges of the swath has been clarified, with the addition of the sentence “OMI pixels broaden in the across track direction as the viewing angle moves away from nadir”.

Page 4, Line 17: *Can you give uncertainties in satellite VCD's? These can be quite large.*

Response

Uncertainties in the satellite VCD's are provided in the data files from the satellite retrievals, and could be shown. However, the figures in the present paper are already quite busy, and the focus is on AMF uncertainties in the iDOAS and satellite measurements (which, as shown in the response to reviewer 3's comments, we feel may be more uncertain than previously thought) and variability within each satellite pixel. We feel that trying to show too much will detract from this focus.

Page 4, Line 20: *I got confused here as on initial reading it sounded like the TM₄NO₂A was OMI data but with SCIAMACHY stratospheric slant columns as strat columns had just been mentioned.*

Action

The sentence has been changed to: “The TM₄NO₂A product is a product using slant column measurements from the SCIAMACHY satellite instrument and a similar scheme using model profiles and stratospheric columns from the TM₄ model.”

Page 4, Line 26: *Suggest mentioning swath width here and how many across track pixels there are here.*

Action

This has been added to the improved description of the DOAS measurements earlier in the section.

Page 5, Line 12: Why do you average to 1.2 km? If purpose is to examine intra-pixel variability, how much cross-track and along-track information are you losing? Is this done to reduce error from noise?

Response

This is in fact a time-based average (10 second moving average), which at the flight speed works out to approximately 1.2km. The iDOAS has 32 across-track pixels, we use only pixel 15 (counting from 0) in this paper.

Along-track averaging is used to reduce noise, for example an earlier version of Figure 7, without the averaging, and using a fixed AMF rather than attempting to quantify iDOAS AMF uncertainty is shown below.

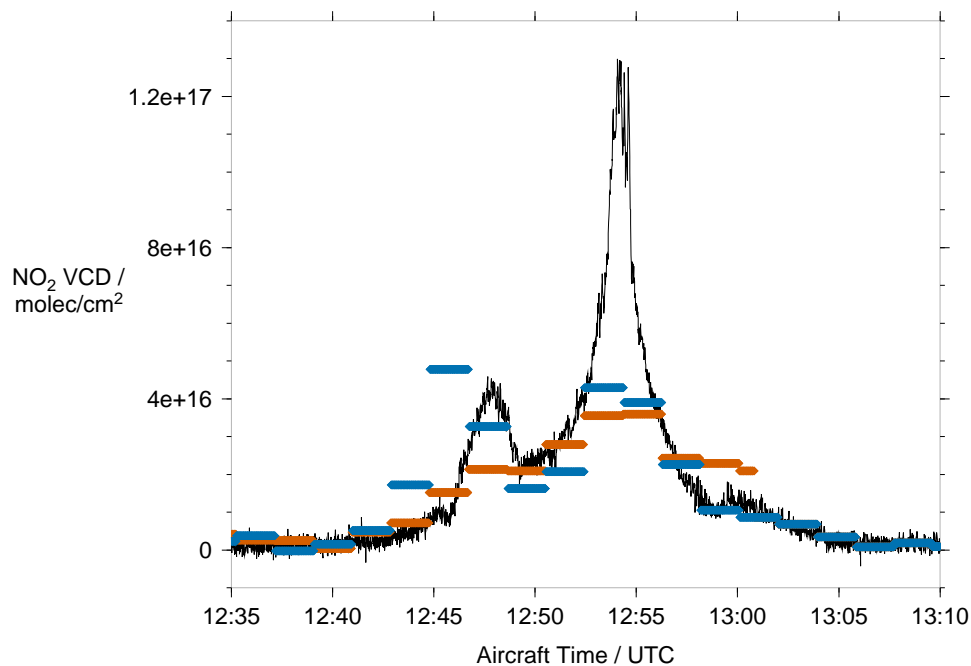


Figure 1: Airborne iDOAS measurements at full resolution (i.e. approx. 80m) on 9 August 2007 compared with OMI DOMINO V2 at aircraft nadir (orange) and one pixel upwind of (blue). A fixed AMF of 1.6 is used for the aircraft measurements in this figure.

Action

In the section on comparing DOAS measurements to the satellite (p5, line 9, which has now been moved under the appropriate sub-heading) the following has been added: “...the first is to average 80m-resolution nadir iDOAS measurements using a ten-second moving average in order to smooth out

fine-spatial-scale variations and make a comparison with the much larger satellite pixels.” and “The second approach is to calculate the mean and standard deviation of all nadir iDOAS measurements . . .”

Page 6, Line 2: Are there only 8 profiles total and what are locations? Maybe mention here to put in context. This intro to the section is a bit confusing as it presents the conclusion all of a sudden without referencing the data/figures. Maybe add an introductory sentence to ease into the analysis.

Response and action

Yes there are only 8 profiles. An introductory sentence has been added: “During each of the flights, a vertical profile measurement was performed before and after the satellite-tracking portion of the flight.”

Page 6: Is the representation of some profiles as exponential valid in this region? Do you have any surface observations, or model profiles to check against? I realize this is done for constraining the error more than anything, so probably doesn't make a big difference, but I'm just curious.

Response

We don't have any model profiles that we feel will be helpful. The state of modelling in South Africa is poor, mostly relevant to regulatory compliance. There are some other unpublished vertical profiles from other campaigns, but we chose to use only those from the 2007 iDOAS campaign. Near to surface sources, and at the spatial scale of the iDOAS, an exponential profile seems more appropriate. This is difficult to confirm, even with an aircraft profile measurement, since aircraft will typically climb and descend in a racecourse pattern, with straight portions of two minutes' flying between 180° turns, amounting to almost 10km of flying. Perhaps an ex-military pilot would be willing to fly more aggressively to make the horizontal extent of vertical profile measurements smaller. This would also require greater coordination with air-traffic control, who might find this sort of maneuvering unusual. A vertical profile climatology would be useful over the Highveld and in fact most regions of the world.

Figure 2 and 3: Can you specify surface altitude here or show on figure? Is it the bottom of the y-axis?

Response and action

Surface elevation at Richards Bay is sea level, and at Nelspruit the aircraft landed to refuel, so the profile is measured down to the surface. This information has been added to the captions and the text.

Figure 4 and relevant text: What do you do for NO₂ profile in stratosphere in the model? Does NO₂ in the stratosphere contribute to the AMF or do you assume it cancels perfectly with the reference spectrum?

Response

We assume that the change in stratospheric AMF during the course of a flight is small, and hence we assume that the stratospheric column cancels with the reference spectrum.

Section 5: Could increase readability with subsection headings here.

Subheadings have been added to separate the descriptions of flight on different days.

Page 12, Line 11: Clearly the AMF changes drastically with the surface albedo. You are using your calculated AMF values to set bounds on the AMF error. How is the uncertainty in the AMF from uncertainty in the albedo determined (it's going to be high, with such a low resolution OMLER product)? Why not use MODIS albedo, or MODIS BRDF for an even better representation of the surface for high resolution observations from the aircraft?

Response

Certainly, using a higher resolution albedo or BRDF would improve our calculation of the AMF, since surface properties have a large influence on the AMF. This would be the logical next step in sophistication of the radiative transfer modelling. It would appear that the uncertainty in the AMF from the profile shape is more important, and more difficult to quantify.

Page 15, Line 15: I found this confusing. What is your reference? Do you have remote ocean measurements from the aircraft?

Response

Reference spectra for our retrieval are chosen from background regions of the flight. Since background regions over land will have a higher column density than remote maritime regions measured by the satellites, we assume that the satellites' measurement of background regions over land are "correct" and we shift the aircraft measurements to match the satellite. This seems reasonable, since background regions have shallow horizontal gradients and the errors in the satellite measurements we describe will be small. This procedure does highlight the problem with using one nadir-viewing scattered-light instrument to validate another. Ideally some other independent measure of vertical column density, with less dependence on *a-priori* profile shape should be used as a reference for both the aircraft and satellite measurements.

Page 14, Line 14: Could the same effect be achieved by putting the iDOAS on an aircraft that flies higher?

Yes, a wider swath could be achieved by flying higher.

Page 14, 19: *“Underestimates” the peak only. What it’s actually probably doing is just averaging out everything in the field of view (so you could equally say “overestimates the background”).*

The regression line is fitted through iDOAS data that is averaged (along track) to the resolution of OMI, hence we are not comparing the peak iDOAS to OMI but rather a 1-dimensional spatial average.

Page 13, Line 5: *Not sure why you have to use two fitting schemes. Does that tell us anything?*

Response

The two fitting schemes attempt to demonstrate that the background measurements by the iDOAS and satellites are a better match than measurements close to sources. However, the reviewer makes a good point: it doesn’t really tell us much.

Action

The inset figure has been removed.

Page 15: *You make a few comments about plume age, source etc. I noticed you used HYSPLIT earlier in the paper. Can it tell you anything about these specific cases?*

In cases where HYSPLIT proved to be useful for plume age estimates, this has been added to the discussion.

Page 16, Line 19: *Can you remind us of SCIAMACHY overpass time here? Also Figure 13 caption reads a bit like the times are for the satellite observations (I’m guessing it didn’t take 50 minutes to fly over the region!)*

SCIAMACHY overpass times are shown in Figure 13 in each SCIAMACHY pixel. The approximate overpass time has been added to the caption.

Page 17, Line 6: *Not sure you can draw any conclusions about SCIAMACHY vs OMI at all here. There is a very limited amount of SCIAMACHY data at high NO₂ values. Obviously your slopes are very different on different days with OMI as well.*

True. We have edited the text appropriately to indicate that no real conclusion can be drawn.

Fig 6 and similar: *Can you specify that these are 1.2 km averages in caption or in text (which I’m assuming they must be?)*

Yes these are 1.2km averages. This can be added to the caption.

Figure 6: *I can’t tell which is sub-aircraft pixel as it looks like flight was right down the border of two cross-track positions. Can you clarify this in*

text?

Yes, the flight track does cross from one OMI-row to the next. This has been clarified in the description of the figure.

Figure 7 and similar, and relevant text: *The average isn't technically over the "area" of the OMI pixel, which might have a 13x24 km² size. Clarify.*

Agreed, it is the average of the full-resolution iDOAS measurements (from the nadir iDOAS pixel only) over the length of flight track within the OMI pixel. The captions and text have been amended to use the term "line-average".

Figure 7 and similar: *Specify colors for elevation/albedo subplot.*

A description of the colours has been added to the caption.

Figure 8: *Specify which are OMI and which are SCIAMACHY observations (maybe in legend?)*

Yes, specifying which are OMI and SCIAMACHY is a good idea. This has been done.

AMT-2016-366: Responses to Anonymous Reviewer

3

Stephen Broccardo

June 20, 2017

Thank you for your review and comments, which have added substantial value to the paper.

Reviewer comment 1: *Four research flights are analysed and discussed in quite some detail, but the interpretation of differences between airborne and satellite retrievals could go more into depth. Based on the present manuscript, the reader might get the impression that systematic differences in tropospheric NO₂ columns between satellite and iDOAS can be explained solely (or largely) by horizontal variability in the tropospheric NO₂ columns on a scale that is smaller than the typical size of satellite pixels. What would be particularly relevant is to investigate further the potential impact of profile shape assumptions for NO₂ and aerosols in explaining the difference between satellite and airborne measurements over the most polluted regions. Close to major point sources one may expect not only to find locally quite extreme tropospheric NO₂ column abundances, but at the same locations also the NO₂ profile shape may deviate considerably from other places further away from the main sources. In this context, it may be relevant to distinguish explicitly four profiles: the true profile at the spatial resolution of the aircraft measurements (P true air), the profile used in the airborne retrieval (P prior air), the true profile at the resolution of the satellite measurements (P true sat) and the profile used in the satellite retrieval (P prior sat). Differences in tropospheric NO₂ column retrievals (space-borne vs airborne) cannot be interpreted without taking into account these four profile shapes in the discussion. How much do the authors think P true air can deviate from P prior air close to the main sources (same for P true sat and P prior sat). Furthermore the AMF is not only affected by the (different) profile shapes, but also by the block-AMFs, and these are not identical for the satellite and the airborne point of view. This should be taken into account as well.*

Despite the length of this comment, I would suggest to add just one or two paragraphs addressing this point and providing some first order estimates. It would for instance be enlightening to the reader if the impact of making

wrong profile shape assumptions is worked out for one hypothetical scenario. For instance (it is up to the authors to deviate from this concrete suggestion): scale height for P true air is 0.2km (e.g. close to strong isolated source); scale height for P true sat is 0.4km (averaged over a larger region the true profile is less dominated by the local source); scale height for P prior air is 0.6km (this number is used in the present study); scale height for P prior sat is taken from the profile used in DOMINOv2 product over this region. Block AMFs should be applied for a representative SZA and surface reflectance. When combined, this information should provide the reader with a first order quantitative estimate of local AMF fluctuations near a strong plume: to what extent can this explain the discrepancy between the satellite and airborne retrieval? Or perhaps it is concluded that - when taking this effect into account - the observed discrepancy increases even further.

Response

This is a good idea. We have developed a further suite of vertical profile scenarios, based on Scenarios 11 and 12. These scenarios have a variety of scale-heights from 0.2km to 1.4km.

Like in the previously presented model scenarios, AMFs were calculated for each profile shape with all the permutations of SSA set at 0.82, 0.90, and 0.98; and surface albedo set at 0.02, 0.05, 0.08, and 0.11. All these profiles, like their parent profiles of scenario 11 and 12, have the surface elevation set to 1400m. In order to address the reviewer's next comment pertaining to the use of a fixed AOT, calculations were repeated with the AOT set to 0.1, 0.3 and 0.5.

What is remarkable from Figure 1 in this response, is that the trend in AMF with decreasing scale-height is negative for scenarios without an elevated layer, and positive for scenarios with such a layer. Such layers have been observed in this and other measurement campaigns. This result implies that close to a surface NO₂ source, such as the city of Johannesburg, the error from incorrect choice of *a-priori* vertical NO₂ profile cannot be determined without an actual profile measurement.

Action

The following paragraphs and the figure have been added to the discussion on page 14:

It is instructive to evaluate the potential air-mass factor error that might be made by assuming an incorrect vertical profile of NO₂. Several more radiative-transfer modelling scenarios are introduced, based on scenarios 11 and 12, i.e. with an exponentially-decreasing profile, surface elevation set at 1400m, some profiles with an elevated layer of NO₂ and some without. The scale height of the profiles is varied from 1400m to 200m, and radiative

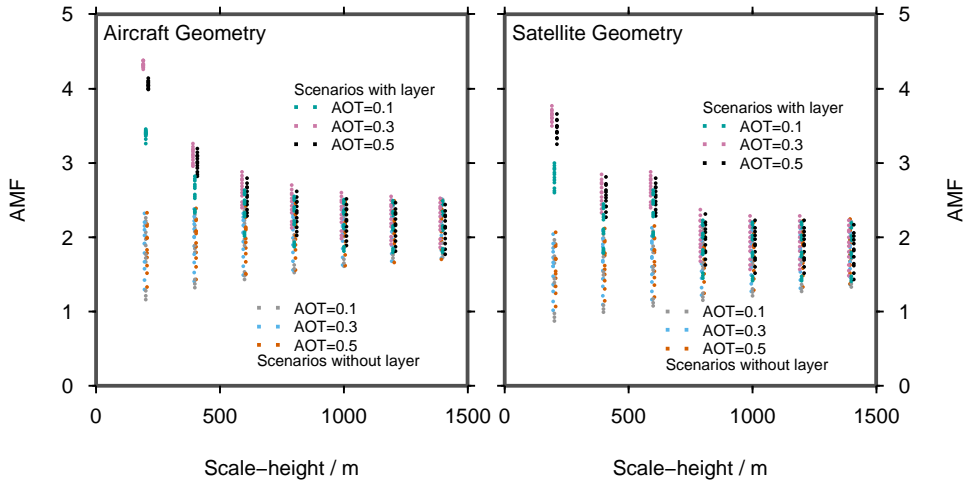


Figure 1: AMFs for scenarios of varying scale-height, for aircraft viewing geometry (left) and satellite viewing geometry (right). For each scenario of scale-height and AOT, variability in the AMF is due to variations in surface albedo and single-scattering albedo.

transfer calculations are done at a representative solar zenith angle of 55° . Once again air-mass factors for permutations of AOT of 0.1, 0.3, and 0.5, and SSA of 0.82, 0.90, and 0.98 are calculated. Results for aircraft- and satellite viewing geometry are presented in Fig. 8. It can be seen that the AMF increases for scenarios with an elevated NO_2 layer as the vertical profile scale-height is decreased. In contrast, the AMF for scenarios without such a layer decreases as the scale-height is reduced. In the satellite viewing geometry, the behaviour is slightly different, with a flattening off of the AMFs with scale-heights of 600m and 400m, compared to the aircraft viewing geometry. This behaviour can likely be explained by examination of the block-AMFs for the two cases, however such analysis is beyond the scope of the present study.

We might estimate the VCD error arising from AMF uncertainty for the iDOAS using two profiles: the true profile at the spatial scale of the instrument, P_{true} and the profile used in the AMF calculation P_{prior} , along with the associated AMFs: AMF_{true} and AMF_{prior} . If P_{prior} is an exponentially-decreasing profile with scale-height of 1000m either with- or without an elevated layer, AMF_{prior} will lie between approximately 1.6 and 2.6. Close to a surface source of NO_2 P_{true} might have a much smaller scale-height, for example 400m. In the case of a profile with an elevated layer, AMF_{true} should be between 2.5 and 3.2. Using the mid-points of the uncertainty ranges of AMF_{true} and AMF_{prior} , this will lead to a 26% overestimation of the VCD. In the case of P_{true} having no elevated layer, AMF_{true} will lie between approximately 1.2 and 2.3, leading to a 20% underestimation of the

VCD from the use of AMF_{prior} .

In the case of a satellite measurement, a representative profile for the satellite pixel is likely to have a larger scale-height, since more background areas will be included in the measurement along with the surface source and the discrepancy between AMF_{prior} and AMF_{true} will be less, but will behave in a similar manner to that described above. This highlights the need for an improved P_{prior} as the spatial resolution of the measurement improves.

Reviewer comment 2: *Although aerosols are not entirely neglected in this study, they receive little attention considering the fact that for all four flights - each covering distances of hundreds of kilometers - just one fixed value is assumed for the AOT. It is quite remarkable that the uncertainty range of the AMF is derived using a look-up table that does include variability of the single-scattering albedo, but not of the AOT. Over a region where the variability in NO_2 is so large, it is almost unthinkable that the AOT can be approximated with a single value. To some extent the same argumentation as given above (in the vicinity of a strong pollution source the NO_2 profile shapes may show considerable spatial variability) can be given here as well: in the same region the AOT may show a substantial variability (although probably less extreme than for NO_2). In my opinion this point should at least be mentioned. It would be even better to find satellite AOT data (e.g. from MODIS) for the days of the research flights to provide more insight into the relevant parameter*

Agreed. The approach taken to constrain AMF uncertainty arising from profile shape, SSA, surface albedo, surface elevation and SZA in this paper, by calculating all the permutations of these parameters, is extended to the AOT. The above parameters are further permuted with AOT's of 0.1, 0.3 and 0.5. 2-dimensional plots of AMF vs SZA (which could be thought of as slices of the discussion paper's Figure 5) are shown below for each surface albedo, with the original modelling highlighted in orange, and the additional permutations with the and lower and higher AOT in grey and blue-green respectively.

The increase in the range of AMF uncertainty derived from the present approach of modelling all permutations, as a result of the extra two AOT's used is not as large as might be anticipated. Nevertheless, the new values of minimum and maximum AMF will be used and figures, tables and discussion in the manuscript will be updated. In addition, a mistake in scenario 12, where the incorrect vertical profile of NO_2 was used, has been corrected.

Reviewer comment 3: *In the manuscript the discrepancies found between *i*DOAS and OMI (SCIAMACHY) are not compared to results from other validation studies, e.g. where OMI retrievals are compared to MAX-DOAS observations. In the last years many of such studies were doen, with MAX-*

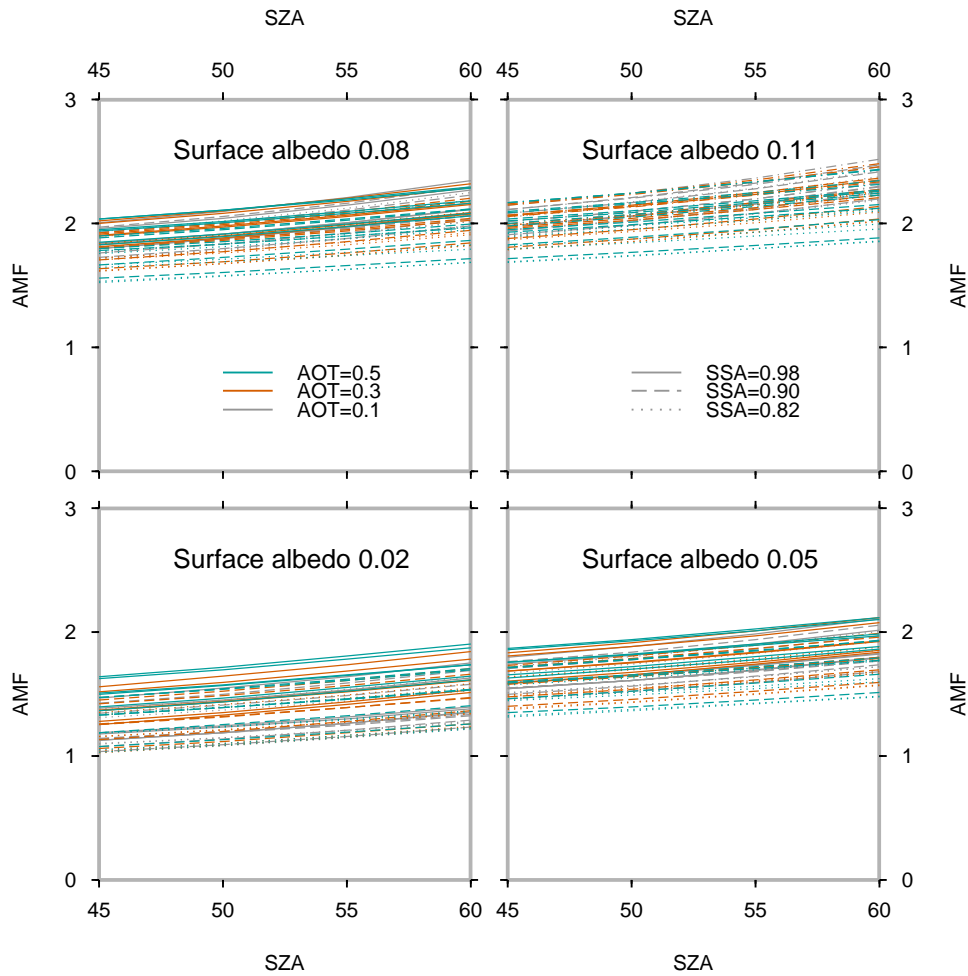


Figure 2: AMF versus SZA plots at different surface albedo's for scenarios with the surface elevation at sea level. AOT=0.3 (as in the discussion manuscript) is plotted in orange, and the additional scenarios of AOT=0.1 and 0.5 are plotted in grey.

DOAS instruments either in rural or in urban regions. It would be valuable to link the findings of this study to findings in such inter-comparisons.

Response and Action

The following paragraph has been added:

Comparison studies of ground-based multi-axis DOAS (MAX-DOAS) instruments with satellite measurements have given mixed results. Some studies (Irie et al, 2008; Hains et al 2010) showing MAX-DOAS results consistently lower than OMI. Kanaya et al (2014) shows DOMINOv2 biases of up to 50% lower than the MAX-DOAS, although the bias improves when only

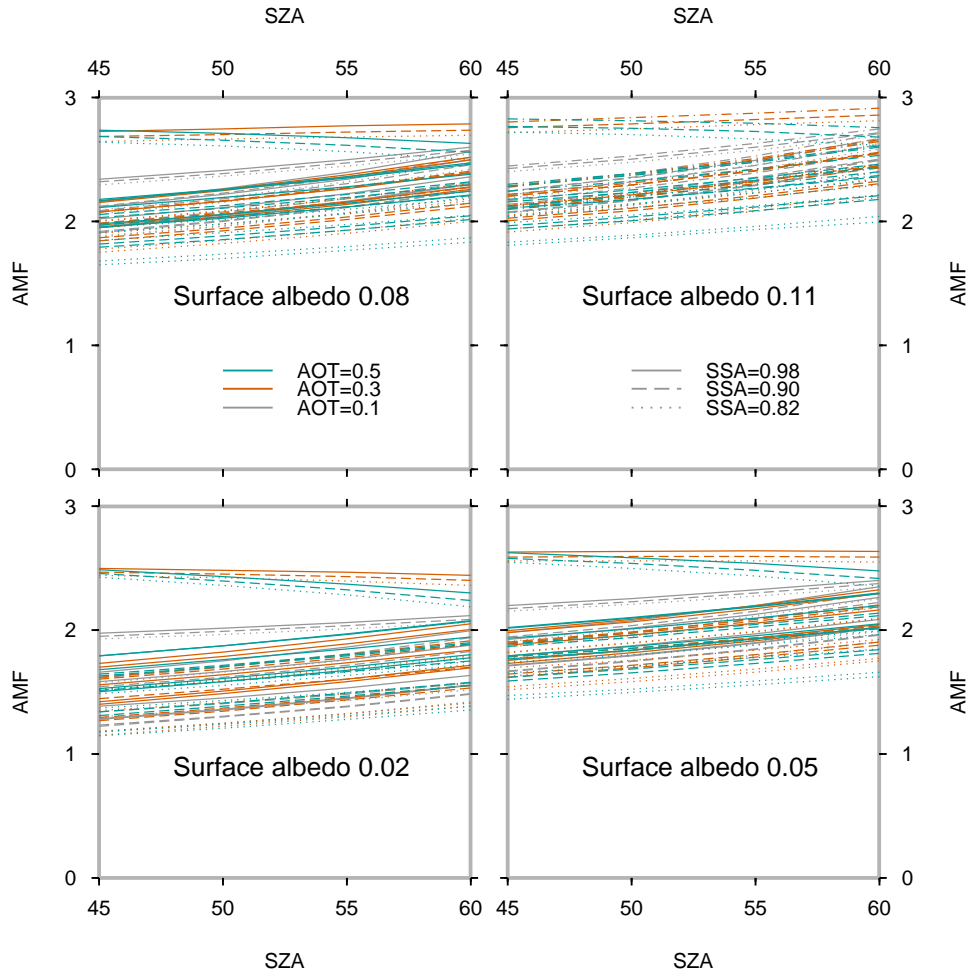


Figure 3: AMF versus SZA plots at different surface albedo's for scenarios with the surface elevation at 1400m above sea level. AOT=0.3 (as in the discussion manuscript) is plotted in orange, and the additional scenarios of AOT=0.1 and 0.5 are plotted in grey and blue-green respectively.

remote surface sites are considered. This is attributed to both horizontal inhomogeneity within the OMI pixels and the inability of OMI to observe NO_2 close to the surface.

Reviewer comment 4: *On section 2: please provide some more details on the iDOAS observations. For instance: the field of view, number of pixels in across-track direction.*

Reviewer comment 5: *I am missing a formula that describes how VCD's are derived precisely from the (differential) slant column measurements. In my opinion, this should be described in more detail, although it has already been described elsewhere in full detail.*

Response

These two comments are similar to comments made by Reviewer 1. Details of the iDOAS and the retrieval have been expanded.

Reviewer comment 6: *The statements in Sect 3 are quite general. The words "usually" (p.3,l.3) and "frequently" (p.6,l.8) suggest a large number of profiles that are measured. However, these are not shown. Furthermore it is not clear if the profiles that are measured are representative for the plume or for more remote regions (see also the first comment).*

Response

It is true that these words express more confidence than what is warranted by the limited number of profiles measured during this campaign. The confidence that the authors feel is not from the profiles measured at the start and end of each iDOAS-measurement flight leg, which frequently were in background conditions; but rather from the literature on stable discontinuities over the Highveld, which is based on an analysis of long-term observations, and on how in the literature, elevated trace-gas and aerosol layers are frequently associated with these stable discontinuities, an observation corroborated by our own measurements. The impact of the presence or absence of such layers on the AMF has emerged as a finding of the present study, discussed above in the response to the reviewer's first comment.

Action

The language has been changed to reflect the above discussion.

Reviewer comment 7 *Figure 5 could be better readable if a grid was plotted on the left and right side of each cube. Furthermore it could be beneficial to use colours instead of different line styles and to provide a legend.*

Response

This was attempted, however the increased clutter in the diagram made it even more difficult to read.

Action

The 3-d figure will be replaced with the conventional plots shown in response to point 2 above. A 3-d figure will be retained to illustrate the principle of a minimum- and maximum-AMF plane.

Reviewer comment 8: *P.15, l24-25: "... indicating that ... 9 Aug". The terminology 'aged' versus 'young' might cause confusion, as some readers might wrongly think of 'photochemical aging'. It might be that what is here called an 'aged plume' is actually a region where the NO₂ profile is less shallow than for a 'young plume', and more in line with the prior NO₂ profile shape used for the OMI and/or iDOAS retrievals (see also the first*

comment). If this is the case, then one cannot say that OMI would be limited in its ability to capture the higher NO₂ gradient in the young plume because it is 'young'; for instance it could be more appropriate to say that the AMF derived using the prior profile shape used in the DOMINO product better matches the profile shape of an aged plume than the profile of a young plume. Please comment on this.

Response

Indeed, the terminology may cause confusion. What is implied by an “aged” plume is one that is more dispersed in both the vertical and horizontal directions. The shallower horizontal gradients in a more dispersed, “aged”, plume are one reason why OMI might be better able to observe a more representative VCD, since the horizontal distribution of NO₂ across the OMI pixel is more homogeneous. This is what was meant in the discussion paper.

As the reviewer points out, the vertical dispersion of NO₂ in an “aged” plume could mean that the actual profile shape is closer to the *a-priori* profile used to calculate the satellite AMF. In addition, as shown in the figure above, potential errors in the AMF are less for profiles with a larger scale-height, and the divergence in the sign of the error for scenarios with- and without elevated layer found at low scale-heights disappears. This implies that AMF uncertainty will be smaller further downwind.

Action

The above discussion has been added, and the terminology has been changed.

Intra-pixel variability in satellite tropospheric NO₂ column densities derived from simultaneous ~~spaceborne~~ space-borne and airborne observations over the South African Highveld

Stephen Broccardo¹, Klaus-Peter Heue², David Walter³, Christian Meyer⁴, Alexander Kokhanovsky^{5,6}, Ronald v.d. A⁷, Stuart Piketh⁸, Kristy Langerman⁹, and Ulrich Platt¹⁰

¹School of Geography, Archaeology and Environmental Science, University of the Witwatersrand, Johannesburg, 2030, South Africa, *now at* Climatology Research Group, Unit for Environmental Science and Management, North-West University, Potchefstroom, 2531, South Africa

²DLR Earth Observation Center, Oberpfaffenhofen, 82234 Wessling, Germany

³Max Planck Institut für Chemie, Hahn-Meitner-Weg 1, 55128 Mainz, Germany

⁴IDT Europe GmbH, Grentzstr 28, 01109 Dresden, Germany

⁵EUMETSAT, Eumetsat Allee 1, 64295, Darmstadt, Germany

⁶Moscow Engineering Physics Institute, National Research Nuclear University, Kashirskoe Ave. 31, 115409, Moscow, Russia

⁷R&D Satellite Observations, KNMI, Utrechtseweg 297, 3731GA, De Bilt, Netherlands

⁸Climatology Research Group, Unit for Environmental Science and Management, North-West University, Potchefstroom, 2531, South Africa

⁹Eskom Holdings SOC Ltd, Megawatt Park, Maxwell Drive, Sandton, 2157, South Africa

¹⁰Institut für Umweltphysik, Im Neuenheimer Feld 229, 69120, Heidelberg, Germany

Correspondence to: S. Broccardo (sbroccardo@gmail.com)

Abstract. Aircraft measurements of NO₂ using an imaging differential optical absorption spectrometer (~~DOAS~~ DOAS) instrument over the South African Highveld region in August 2007 are presented and compared to satellite measurements from OMI and SCIAMACHY. In-situ aerosol and trace-gas vertical profile measurements, along with aerosol optical thickness and single-scattering albedo measurements from the Aerosol Robotic Network (AERONET), are used to devise scenarios for a radiative-transfer modelling sensitivity study. Uncertainty in the air-mass factor due to variations in the aerosol and NO₂ profile shape is constrained, and used to calculate vertical column densities (VCD), which are compared to co-located satellite measurements. The lower spatial resolution of the satellites cannot resolve the detailed plume structures revealed in the aircraft measurements. The airborne DOAS in general measured steeper horizontal gradients and higher peak NO₂ vertical column density. Aircraft measurements close to major sources, spatially-averaged to the satellite resolution, indicate NO₂ column densities more than twice those measured by the satellite. The agreement between the high-resolution aircraft instrument and the satellite instrument improves with distance from the source, this is attributed to horizontal and vertical dispersion of NO₂ in the boundary layer. Despite the low spatial resolution, satellite images reveal point sources and plumes that retain their structure for several hundred kilometers downwind.

1 Introduction

Space-based measurements of trace-gases are increasingly being used to monitor tropospheric air pollution (McLinden et al., 2012; Streets et al., 2013), including the identification of major sources missing from public emissions inventories (McLinden et al., 2016) and the quantification of source strengths (Beirle et al., 2011). Satellite observations have highlighted the South African Highveld as a region with NO_2 column densities higher than expected from emissions inventories (Martin et al., 2002; Toenges-Schuller et al., 2006), and with an increasing trend (Richter et al., 2005; van der A et al., 2008). To further investigate this phenomenon, a high-resolution imaging differential optical absorption spectrometer (iDOAS) was flown on board the South African Weather Service Aerocommander 690A research aircraft during a dry-season flight campaign over the Highveld in 2007. Results from research flights conducted on the 9th, 11th, 14th and 18th of August 2007 are presented. Aircraft vertical profile measurements of NO_y and aerosols are used to devise several representative scenarios of the vertical distribution of these two species, and a sensitivity study is performed using the SCIATRAN radiative transfer model (Rozanov et al., 2014) to constrain the uncertainty in the air-mass factor. Measurements from the nadir pixel of the iDOAS are compared with operational satellite measurements of NO_2 from OMI (Ozone Monitoring Instrument) and SCIAMACHY (SCanning Imaging Absorption spectroMeter for Atmospheric CHartographY) made on the same day.

The Highveld is a high-altitude plateau in the interior of South Africa (Fig. 1), home to the Johannesburg-Pretoria conurbation and the adjoining industrial towns of Ekurhuleni to the east and Vereeniging and Vanderbijlpark to the south. The latter two along with the petrochemical industry and town at Sasolburg enclose an area known as the Vaal Triangle. The Vaal Triangle is also home to two ~~steelmills~~ steel-mills and a coal-fired power station. To the east of Johannesburg, at Secunda, there is a coal-to-fuel (Fischer-Tropsch process) synfuel refinery, which also generates electricity from coal. Secunda is situated in a region often referred to as the Eastern Highveld or Mpumalanga Highveld; this region is also home to eleven more coal-fired power stations, and several steel-mills. Analysis of a year of ground-based monitoring station data by Collett et al. (2010) indicates that most of the NO_2 on the Highveld is from tall-stack industrial emissions, and has an impact on surface ozone concentrations (Balashov et al., 2014). A combined analysis of satellite and ground-based measurements indicates that the conurbation of greater Johannesburg is also a significant source of NO_2 (Lourens et al., 2012). In between the heavy industries are coal mines to supply fuel to the former, a small town about every hundred kilometers, and farmland or grassland. The Highveld is impacted by biomass-burning sources in the winter season; along with the urban and industrial sources of trace-gases and aerosols, it forms a natural laboratory isolated on a global scale from nearby sources, and controlled by synoptic-scale meteorology (Annegarn et al., 2002).

2 Measurements and Methods

2.1 DOAS

The measurement principle employed to observe NO_2 from satellite, and from our airborne iDOAS instrument is that of differential optical absorption spectroscopy (DOAS), described by Platt and Stutz (2008). As with ~~any absorption spectroscopy~~

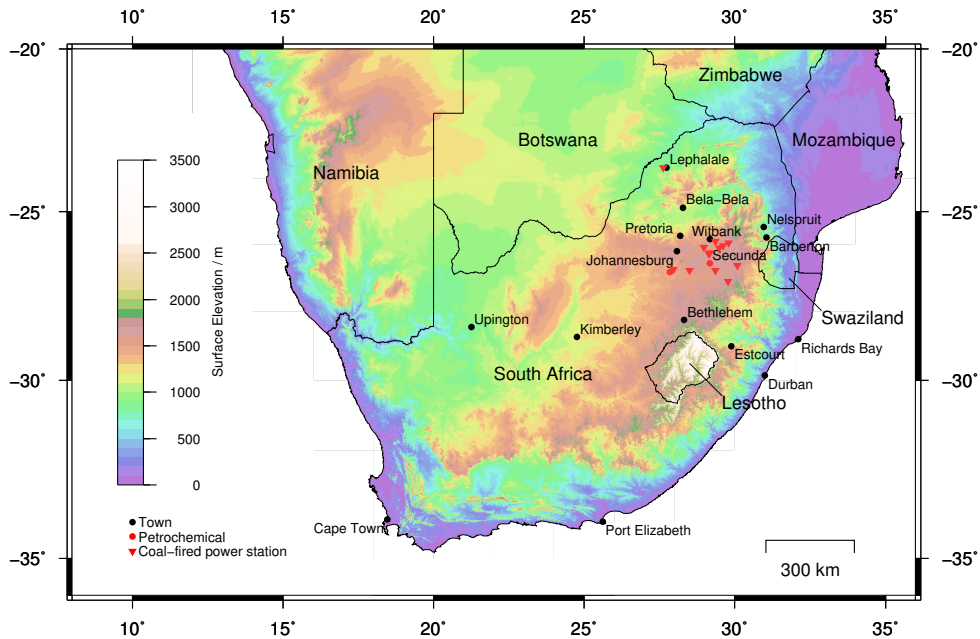


Figure 1. A map of Southern Africa, showing the high-altitude plateau of the Highveld to the east of Johannesburg, and the cluster of coal-fired power stations and heavy industries on the eastern Highveld. The coal-fired power station at Lephale is indicated. Power stations not shown here include smaller coal-fired and gas-turbine power stations operated by the cities.

~~technique~~ many absorption spectroscopy techniques, the magnitude of the measured quantity depends on the path length, p , through the absorber and the ~~concentration, $c(p)$~~ molecular number density, $n(p)$, of the absorber. In the case of measurements made in the atmosphere using ~~scattered~~ sunlight, the DOAS analysis yields a slant column density (SCD), S :

$$S = \int_{\text{path}} c n(p) dp. \quad (1)$$

- 5 This name reflects the fact that the light path through the atmosphere is not known *a-priori*, and to a first ~~geometric~~ approximation, is slanted. A more useful quantity is the vertical column density (VCD), which is the ~~concentration~~ molecular number density of the absorber integrated along a vertical path between the earth's surface and the top of the atmosphere. In the standard DOAS formulation suited to measurement of relatively small slant-column densities (Rozanov and Rozanov, 2010), these two quantities are related by ~~the an~~ air-mass factor (AMF):

$$10 \quad A = S/V \quad (2)$$

where A is the air-mass factor, V is the vertical column density and S is the slant column density as before.

A DOAS instrument based on an ~~Acton 300i~~ imaging spectrograph employing a pushbroom viewing geometry, where each line of pixels across the instrument's swath is captured ~~simultaneously on a CCD device~~ simultaneously on an Andor DU-420BU CCD camera, was fitted into the Aerocommander 690A ~~and slant column~~ research aircraft. This CCD has 255 pixels in the

across-track dimension and 1024 pixels in the spectral direction. The temperature of the spectrograph was kept stable at 30°C using a thermostatic heater in an insulated box, and the CCD temperature was set at -20°C using its own in-built thermo-electric cooler. Eight spectra were co-added into 32 across-track pixels, each with an across-track footprint of approximately 70-80m, assuming a flight altitude of 4500m above the ground. This was done in order to make optimum use of the optical resolution of the instrument. Along-track resolution is determined by the aircraft speed and the integration time of the instrument, which was adjusted automatically in-flight to avoid saturation of the CCD, but is generally about 100m (Heue et al., 2008). In the present study only the nadir pixel of the iDOAS is used.

Slant-column densities were retrieved using the WinDOAS software package, as described in more detail by Heue et al. (2008). Absorption cross-sections for NO₂ (Vandaele et al., 1998), ozone (Burrows et al., 1999), water vapour (Rothman et al., 1998), O₄ (Greenblatt et al., 1990) were fitted across a spectral range of 432nm to 464nm. The Ring effect was accounted for using an appropriate cross-section calculated using the DOASIS software (Kraus, 2006). A reference spectrum was chosen from an appropriate location along the flight track far from known sources implying that slant-column densities from WinDOAS are in fact differential slant column densities. Satellite retrievals use a similar technique, using a measurement over remote ocean areas as an approximation of zero-NO₂. We adjust our slant-column densities using an offset in order to bring the vertical column densities from the iDOAS into line with the appropriate satellite measurement (either OMI or SCIAMACHY) in background areas of our flight track.

Two approaches are taken in order to allow a comparison of the iDOAS with the satellite-based measurements: the first is to average 80m-resolution nadir iDOAS measurements using a ten-second moving average in order to smooth out fine-spatial-scale variations and make a comparison with the much larger satellite pixels. With the aircraft's ground speed being around 120m s⁻¹, on a spatial scale this time-based moving-average is over approximately 1.2km. The second approach is to calculate the mean and standard deviation of all nadir (80m by 100m) iDOAS measurements along the aircraft track within a satellite ground pixel to compare with the value from the satellite tropospheric NO₂ product for that pixel. This is referred to as a line-average.

2.2 In-situ measurements

In addition to the imaging DOAS (iDOAS) instrument, the aircraft carried a Particle Measurement Systems Passive Cavity Aerosol Spectrometer Probe 100X (PCASP), operated with the pre-heater switched on; and a Thermo Scientific 42i chemiluminescence instrument with a molybdenum converter in the cabin, plumbed into the aircraft's scientific-air inlet in order to measure in-situ NO_y. An In such instruments the converter converts NO₂ to NO, which is then measured by chemiluminescence; however a molybdenum converter also converts other nitrogen species which comprise NO_y. This can be avoided using a photolytic converter, however an instrument with a photolytic converter to measure NO₂ was not within the project's budget. The aircraft is fitted with a Rosemount ambient temperature sensor, and a separate pitot-static system for measurement and logging of static and dynamic pressure. The humidity sensor fitted to the aircraft did not function during this campaign. The aircraft's data acquisition system also logged parameters from a GPS (Global Positioning System) receiver.

Aerosol number concentration and in-situ NO_y are averaged into 50m altitude bins, temperature into 20m bins. Altitude intervals of interest are identified by inspection of the vertical profile measurements, and average particle size spectra are calculated. No corrections for aerosol refractive index are made to the PCASP measurements (Rosenberg et al., 2012; Liu and Daum, 2000) since the present measurements are not used for determination of radiative properties of the aerosols.

5 2.3 Satellite measurements

Satellite-based measurements of NO_2 were made operationally from the SCIAMACHY (Scanning Imaging Absorption spectroMeter for Atmospheric CHartographY) instrument on board the European Space Agency (ESA) ENVISAT satellite from March 2002 to April 2012; and from OMI (Ozone Monitoring Instrument) on the National Aeronautics and Space Agency (NASA) Aura satellite from October 2004 until the present. The SCIAMACHY instrument operated in a whiskbroom geometry (where the instrument's field-of-view is scanned from side-to-side across the swath) with eight measurement channels covering the spectral range from 214nm to 2386nm. ~~The ENVISAT satellite~~ ENVISAT orbited at a mean altitude of 799.8km with an orbital period of 100.6min and a repeat cycle of 35 days. Overpass time on the Highveld was around 10:00 local time. In the nadir viewing geometry the ground pixel size is 60km by 30km, and global coverage was achieved every 6 days (Gottwald et al., 2006). The Aura satellite orbits at a mean altitude of 709km, with an orbital period of 98.8min and a repeat cycle of 16 days. The OMI instrument measures wavelengths between 270nm and 500nm in pushbroom geometry with a nadir ground-pixel size of 24km by 13km (Levelt et al., 2006). OMI pixels broaden in the across track direction as the viewing angle moves away from nadir. Overpass on the Highveld is around 14:00 local time.

Measurements from the nadir pixel of the iDOAS are compared with NO_2 tropospheric VCD from the DOMINO (Derivation of OMI tropospheric NO_2) version 2.0 product from the OMI instrument (Boersma et al., 2011) available from <http://www.temis.nl>. *A-priori* vertical profiles of NO_2 from the TM4 global chemistry-transport model (Dentener et al., 2003) are used to calculate tropospheric air-mass factors, and stratospheric NO_2 is estimated by assimilation of slant columns in the TM4 model. The TM4NO2A product (also available from <http://www.temis.nl>) uses ~~a similar scheme, however~~ slant column measurements from the SCIAMACHY ~~instrument are used~~ satellite instrument and a similar scheme using model profiles and stratospheric columns from the TM4 model.

25 2.4 Flight strategy

Flights were planned to approximately follow the nadir track of the satellite (carrying OMI or SCIAMACHY) that would be passing over the Highveld on the day, with the aircraft flying nominally at 6000m above sea level, the actual altitude varying by 1000ft (312m) as demanded by air-traffic rules. Over much of the Highveld, this would be approximately 4500m above the ground, giving ~~the size of the approximately square~~ ground pixels from the iDOAS ~~around~~ approximately 80m by 100m (Heue et al., 2008).

At the beginning and end of the satellite-tracking segment of each flight, a vertical profile measurement of NO_y and aerosols was performed. Vertical profiles were started and ended as low as safety allowed, judged visually to be around 400m–500m above ground level (AGL). The lower altitude limit of vertical profile measurements could be ~~extended~~ safely extended down

to the surface if the profiles were flown overhead a suitable airfield, and the aircraft pilot performed a missed-approach procedure. This would limit the choice of locations for vertical profile measurements, but the quality of the profiles would be improved ~~by extending the measurements down to ground level~~. Intermittent failures of the PCASP probe and the data aquisition acquisition system detract from the usefulness of some of the profiles, and these partial profiles are not presented here. Aerosol
5 ~~number concentration and in-situ are averaged into 50 altitude bins, temperature into 20 bins. Altitude intervals of interest are identified by inspection of the vertical profile measurements, and average particle size spectra are calculated. No corrections for aerosol refractive index are made to the PCASP measurements (Rosenberg et al., 2012; Liu and Daum, 2000), since the present measurements are not used for determination of radiative properties of the aerosols.~~

2.5 AERONET measurements

10 Monthly statistics are calculated for the late-winter season from measurements of aerosol optical thickness (AOT) and single-scattering albedo (SSA or $\bar{\omega}$) taken from an AERONET sun-photometer (Holben et al., 2001) that was situated at the University of the Witwatersrand in Johannesburg during 2007 and 2009. The aircraft vertical profile measurements and sun-photometer measurements are used as guidance in creating a number of vertical profile scenarios of aerosols and NO₂; which are used in a model sensitivity study using the SCIATRAN radiative transfer model (RTM) (Rozañov et al., 2014). The results of this
15 sensitivity study are used to constrain the uncertainty in the air-mass factor for the iDOAS NO₂ measurements.

~~Two approaches are taken in order to allow a comparison of the iDOAS with the satellite based measurements: the first is to average high-resolution iDOAS measurements using a ten-second moving average in order to smooth out fine spatial-scale variations and make a comparison with the much larger satellite pixels. With the aircraft's ground speed being around 120, on a spatial scale this time-based moving average is over approximately 1.2. The second approach is to calculate the mean
20 and standard deviation of all iDOAS measurements within a satellite ground pixel to compare with the value from the satellite tropospheric product for that pixel.~~

3 ~~Aircraft Vertical Profile Measurements of and aerosols~~

3 Aircraft Vertical Profile Measurements of in-situ NO_y and aerosols

During each of the flights, a vertical profile measurement was performed before and after the satellite-tracking portion of the
25 flight. From the measured vertical profiles, several features can be discerned:

1. NO_y and aerosol concentration profile shapes are block-shaped or exponentially-decreasing with altitude.

Since aerosol particles or their precursors, and NO_y, often are emitted from the same surface urban, industrial or biomass-burning sources, the patterns of their dispersal will be similar. A block-shaped vertical profile can be expected under conditions where turbulent mixing causes vertical dispersion in the planetary boundary layer, an exponentially-decreasing profile will
30 occur under conditions of greater atmospheric stability, or close to sources where dispersion has not had an opportunity to take place.

2. There are elevated layers of enhanced aerosol and NO_y concentration, isolated from the planetary boundary layer by a layer of cleaner air.

Swap and Tyson (1999) assess vertical mixing and transport of air parcels between spatially and temporally persistent stable layers over the sub-continent. These stable layers around 850hPa (in coastal areas), 700hPa, 500hPa, and 300hPa (corresponding roughly to 1500m, 3000m, 5800m and 9200m respectively) lead to peaks and discontinuities in the vertical profile of trace-gases and aerosols. Published vertical profile measurements of aerosol scattering coefficient (Magi et al., 2003) and particle concentration (Hobbs, 2003; Swap and Tyson, 1999) from the sub-continent show features consistent with this generalization.

3. The aerosol size distribution is consistent in the lower and upper sections the profile

Since the aerosols in the elevated layers are transported there from the lower layers (Swap and Tyson, 1999; Hobbs, 2003) where they are emitted or formed, the size distributions can be expected to be similar. This similarity in aerosol size distribution through the vertical profile was also found in measurements over Namibia (Haywood, 2003a, b), a region frequently under the influence of the same sub-continental-scale air transport regime as the Highveld (Swap and Tyson, 1999). Assuming that aerosol optical properties are the same in the elevated layers as they are near the surface, similar size distributions mean that the aerosol scattering and absorption coefficients will be proportional to aerosol number concentration. These generalizations of the vertical profile are used to develop scenarios for a ~~radiative transfer~~ radiative-transfer modelling sensitivity study described below.

As examples of aircraft vertical profile measurements, the profile overhead the coastal town of Richards Bay measured on 11 August is shown in Fig. 2 and the profile overhead Nelspruit on the same day is shown in Fig. 3. The lower limit of the former profile was around 500m, the latter profile was measured down to the surface, since the aircraft landed at Nelspruit. Extrapolating the available measurements to the surface at Richard's Bay, the aerosol number and NO_y concentrations appear to follow a generally exponentially-decreasing profile with height. The top of this exponential profile is at the bottom of a temperature inversion around 1750m (approximately 815hPa). Embedded within this profile there is a layer of elevated NO_y between 700m and 1000m; this layer of enhanced NO_y concentration is approximately mirrored in the aerosol profile. In addition to the exponentially-decreasing profile close to the ground there is a separate elevated layer of enhanced aerosol and NO_y , between 2200m and 2700m above sea level, capped by another temperature inversion at approximately 2700m (730hPa). Layer-averaged aerosol size spectra from the altitude intervals 500m–600m, 700m–900m, 1000m–1600m, and 2200m–2700m indicate a similarly-shaped bimodal ~~lognormal~~ log-normal distribution in all cases, with modes at 0.13 μm and 2.25 μm .

Over Nelspruit (Fig. 3), the aircraft descended through a plume between 2900m–2500m, observed to originate from a large forest-fire nearby; NO_y concentrations up to 35ppb and aerosol number concentrations greater than 6000 cm^{-3} were measured in this plume. This large plume was trapped under a temperature inversion at 2900m AMSL (approximately 710hPa). Below this, between 2400m–2100m a layer of enhanced aerosol number concentration, and NO_y concentration was found. From the bottom of this layer to the ground (~~the aircraft landed at Nelspruit to re-fuel~~), the NO_y concentration remains approximately constant, and the particle number concentration shows some variations, but in general a block-shaped vertical profile is found.

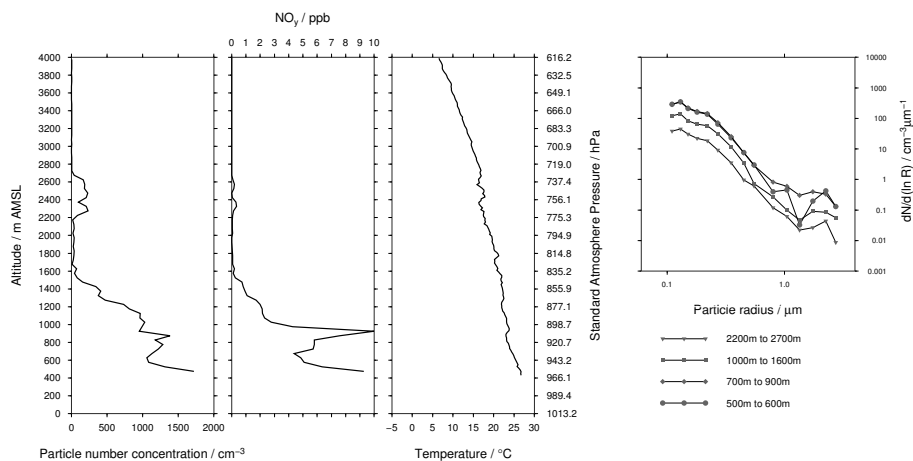


Figure 2. Vertical profiles of particle number concentration, in-situ NO_y and temperature on 11 August 2007 between 11:01 and 11:40 UTC overhead [the coastal town of Richards Bay](#). Average particle size spectra for altitude intervals of interest are plotted.

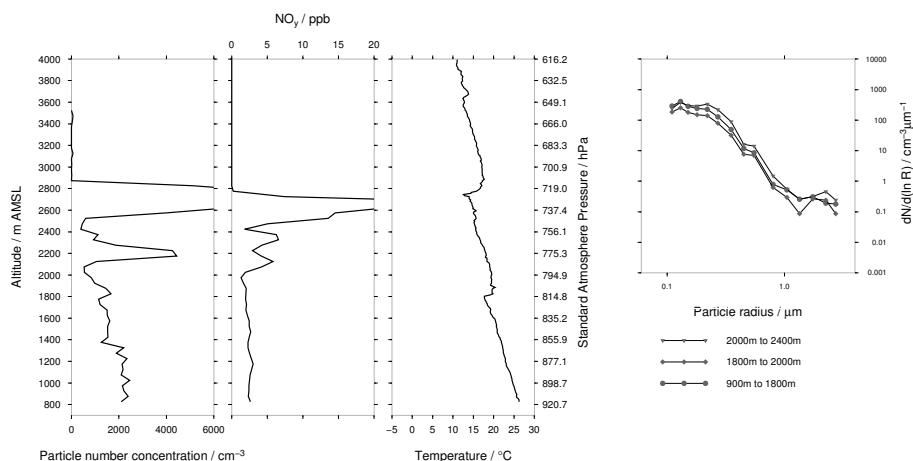


Figure 3. Vertical profiles of particle number concentration, in-situ NO_y and temperature on 11 August 2007, overhead Nelspruit between 12:40 and 13:20 UTC. [The aircraft landed at Nelspruit, so the profile is measured down to the surface](#). Average particle size spectra for altitude intervals of interest are plotted. The elevated layer between ca. 2900–2500m is due to a large forest fire plume.

Aerosol size spectra for the intervals between and 900m–1800m, 1800m–2000m and 2000m–2400m indicate a bimodal log-normal size distribution with the modes of the distribution at $0.13\mu\text{m}$ and $2.0\mu\text{m}$.

Seventy-two hour Hysplit (Stein et al., 2015) back-trajectories (not shown here) indicate that the air measured in these profiles had re-circulated over Mozambique, southern Zimbabwe and south-eastern Botswana before making its way in a south-easterly direction towards either Richards Bay or Nelspruit.

4 Radiative Transfer Modelling and Airmass Factor Calculation

It is ~~obvious-clear~~ that the optical properties of aerosols need to be included in the calculation of the air-mass factor (AMF, defined in Section 2) as highlighted by Leitão et al. (2010). In that study, several vertical profile scenarios are devised from chemistry-transport model output. For the present study, idealised scenarios representative of the Highveld are used to perform a sensitivity study using the SCIATRAN radiative transfer model (Rozanov et al., 2014). Our scenarios are based on two archetypal profile shapes: a block-shaped profile where the concentration of aerosols and trace-gases is constant up to a certain height, and a profile where these concentrations decrease exponentially with height.

Table 1. A summary of AERONET Level 2.0 sun photometer measurements of daily-average aerosol optical thickness at 440nm at the University of the Witwatersrand in Johannesburg during late winter 2007, 2009, and 2011.

| | | AOT | | |
|------|------|------|------|------|
| | | 2007 | 2009 | 2011 |
| July | Min | 0.08 | 0.06 | 0.17 |
| | Mean | 0.14 | 0.11 | 0.25 |
| | Max | 0.20 | 0.18 | 0.30 |
| Aug | Min | 0.22 | 0.14 | 0.12 |
| | Mean | 0.26 | 0.17 | 0.18 |
| | Max | 0.31 | 0.23 | 0.27 |
| Sept | Min | 0.26 | 0.27 | 0.07 |
| | Mean | 0.28 | 0.34 | 0.11 |
| | Max | 0.30 | 0.46 | 0.15 |

Measurements of aerosol optical thickness at 440nm (AOT), and retrievals of aerosol single-scattering albedo at 441nm (SSA or $\bar{\omega}$) over the Highveld are available in the AERONET Level 2.0 dataset from the sun photometer that was situated at the University of the Witwatersrand in Johannesburg during 2007, 2009, and 2011. Daily-mean statistics of these measurements are summarised in Table 1. The intention is not a detailed analysis of the AERONET record, but rather to determine reasonable AOT and $\bar{\omega}$ magnitudes for input into the radiative transfer model. Monthly-mean values of AOT for August are between 0.17 and 0.26 for the three years, however examining the data as a time-series (not shown here) we find that days with higher daily-mean AOT are associated with higher ~~variability-variability~~ within that day, with values greater than 0.5 on some days. These high AOT values are likely associated with SO₂ plumes ~~Laakso et al. (2012)~~ (Laakso et al., 2012) from industrial and household combustion processes which are also NO₂ sources. Biomass burning is also a source of both NO₂ and aerosols ~~Maenhaut et al. (1996); Eck (2003)~~ (Maenhaut et al., 1996; Eck, 2003), hence we choose ~~a representative AOT of 0.3, on the high side of the daily-mean value~~ representative aerosol optical thicknesses of 0.1, 0.3 and 0.5 and scale the vertical profile of scattering and absorption coefficients in our model runs appropriately. SSA retrievals are scarce in the Level 2.0 dataset, with

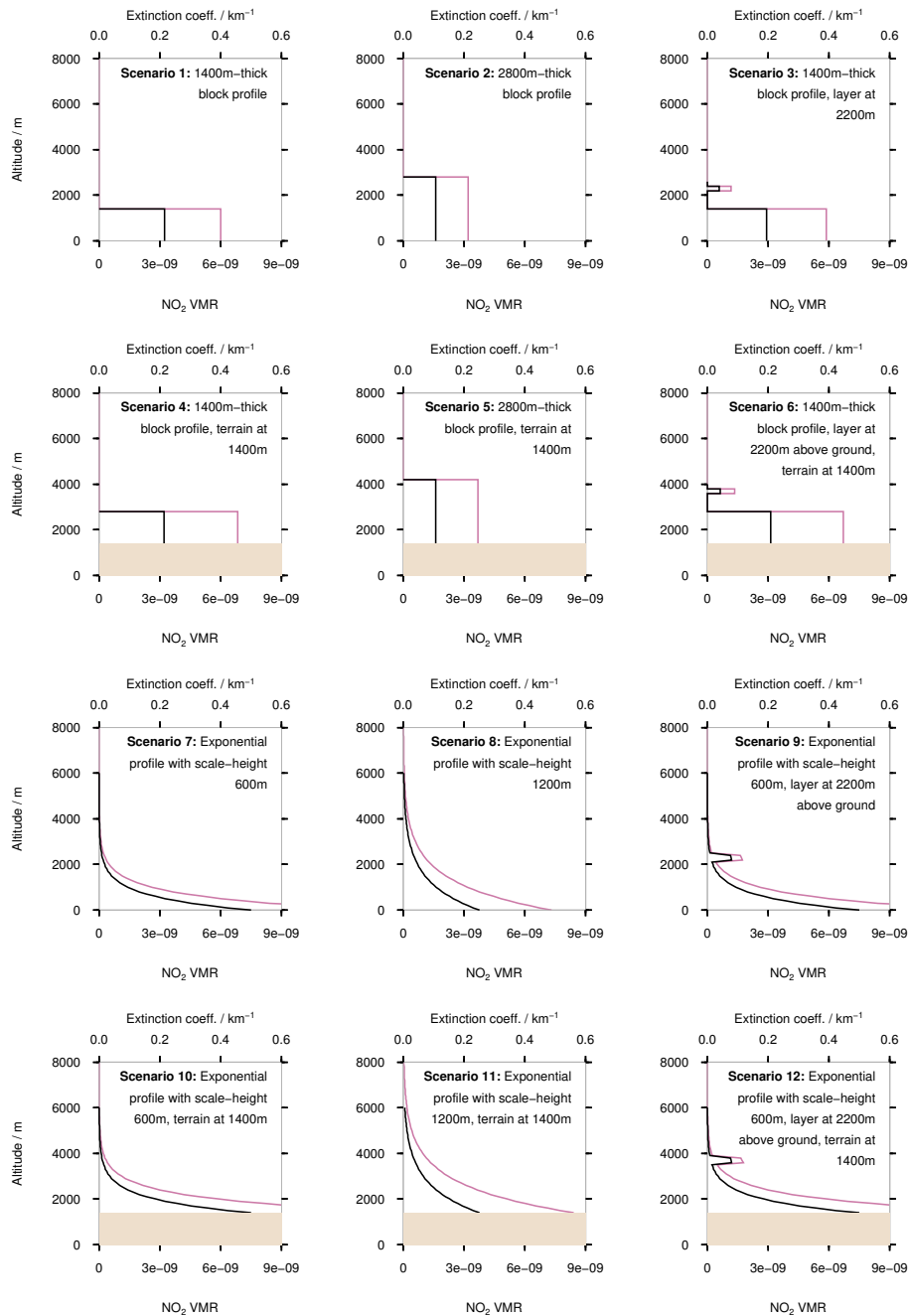


Figure 4. Profile shapes of aerosol extinction coefficient (black line) and NO₂ mixing ratio (purple line) for the twelve scenarios used in the radiative transfer model sensitivity study. The scenarios are designed to all have the same ~~AOT~~ and NO₂ VCD. Extinction and absorption coefficients are scaled to produce aerosol optical thicknesses of 0.1, 0.3, and 0.5. Terrain height is indicated by the shaded light-brown area. Note that the vertical grid used in the model extends up to 10000m

no retrievals in 2007 during these months, and only three in 2009 ranging between 0.83 and 0.88. In 2011, the SSA values for the months of July to September ranged from 0.87 to 0.99.

Unlike the study of Leitão et al. (2010), wherein vertical profiles representative of urban and rural scenes with different VCD and AOT values were used, the present idealized scenarios are designed to all have the same ~~AOT of 0.3, and the same~~ NO₂ VCD of 20 petamolec cm⁻² (2×10^{16} molec cm⁻²), and as mentioned above AOT values of 0.1, 0.3 and 0.5 are used. The NO₂ volume mixing ratio (VMR) between the top of the block, and either the elevated layer above, or the top of the model grid is set at 1.0×10^{-11} (10ppt), in order to avoid undefined block-AMFs in these parts of the vertical grid (a block-AMF is similar to an AMF, but for a subset of the total vertical column). Scenarios are introduced where an elevated layer of aerosols and trace gases are added to the profile shape, as has been observed during this and other field campaigns in the region. Since large portions of the Highveld are at altitude, the effect of a change in surface elevation from sea-level to 1400m above sea-level is evaluated. The twelve model scenarios' profile shapes are shown in Fig. 4.

The radiative transfer model (RTM) is run at a wavelength of 440nm, with the surface albedo set at 0.02, 0.05, 0.08 and 0.11. The solar zenith angle is varied from ~~25~~45°–60° in steps of 5°. Aerosols are modelled using representative single-scattering albedos ($\bar{\omega}$) of 0.82, 0.90 and 0.98; and a Henyey-Greenstein phase function with an asymmetry parameter of 0.7 (Henyey and Greenstein, 1941). An altitude grid of 200m-thick layers from the surface up to 10000m is used. The aircraft altitude is fixed at 6000m above sea level in all scenarios. For the satellite viewing geometry, the observer is placed at the top of the altitude grid. Lambertian surface reflectance is assumed.

Calculated AMFs are summarised in Fig. ~~7: at the two surface elevations modelled (i. e. 0m~~ 5 for scenarios with the surface elevation at sea-level, and in Fig. 6 for the scenarios with surface elevation at 1400m above sea-level. In both figures, results from model runs with the AOT set at 0.3 are plotted in orange; runs with AOT of 0.1 and 1400m), AMFs 0.5 are in grey and blue-green respectively. Calculated AMFs at 0m surface elevation are summarised in Fig. 7: AMFs appear to be constrained between a minimum- and maximum-AMF surface. A similar plot for the results at 1400m would similarly constrain the AMFs between two surfaces. For a given combination of altitude, SZA and surface albedo, variation in the AMF is due to variation in the trace-gas and aerosol profile shapes, AOT, and aerosol single-scattering albedo. From the results shown in Figs. 5 and 6, it would appear that the influence of AOT on the range of likely AMFs for a given SZA and surface albedo is less than the combined influence of profile shape and SSA. Increased surface elevation broadens the uncertainty range. Although these scenarios are by no means exhaustive, they are representative of what is frequently may be found in the atmosphere above the Highveld, and allow the uncertainty in the AMF to be constrained.

5 Airborne DOAS measurements

The high spatial resolution (around 80m) aircraft-nadir measurements from the iDOAS (Heue et al., 2008), when combined with a flight path following the satellite track, might be thought of as giving a transect of each satellite ground pixel. Two approaches are taken in order to make a comparison between measurements from the two platforms: a time-domain moving-

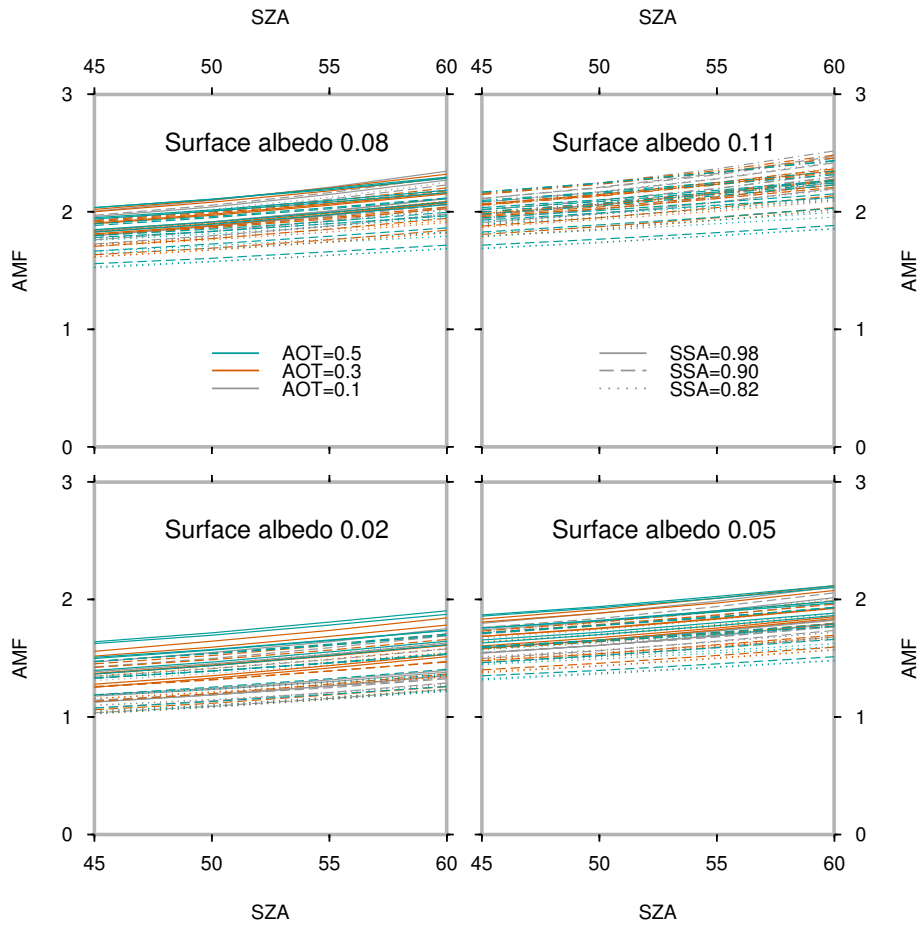


Figure 5. Calculated air-mass factors from the twelve six low-surface-elevation (sea-level) scenarios outlined in Fig. 4, plotted as a function function of solar zenith angle and surface albedo for the high-surface-elevation scenarios (top) and sea-level scenarios. A dotted line indicates $\bar{\omega}=0.82$, a dashed line $\bar{\omega}=0.90$ and a solid line $\bar{\omega}=0.98$. In general, an increase in AMF with increasing single scattering albedo AOT is found. Variation in the AMF due to variations in aerosol properties and vertical profile shape are bounded indicated by a minimum line colour: grey for AOT=0.1, orange for AOT=0.3, and maximum AMF surface at each surface elevation blue-green for AOT=0.5.

average of the aircraft VCD measurement and a spatial average line-average of the high-resolution aircraft measurements within each satellite pixel.

Variability in the AMF for the aircraft measurements is constrained between the minimum- and maximum AMF surfaces described above in relation to Fig. 7. In order to determine the maximum- and minimum AMF, and hence the uncertainty
 5 in the VCD due to the aerosol profile shape in the vertical column density profile shape and aerosol properties, successive linear interpolations between data points along SZA, surface albedo, and surface-elevation axes are performed for each iDOAS measurement. Solar zenith angle is calculated from for the aircraft time and position using the pyEphem package (Rhodes, 2015). Surface albedos are sampled from the OMI albedo climatology (Kleipool et al., 2008), hence the spatial resolution of

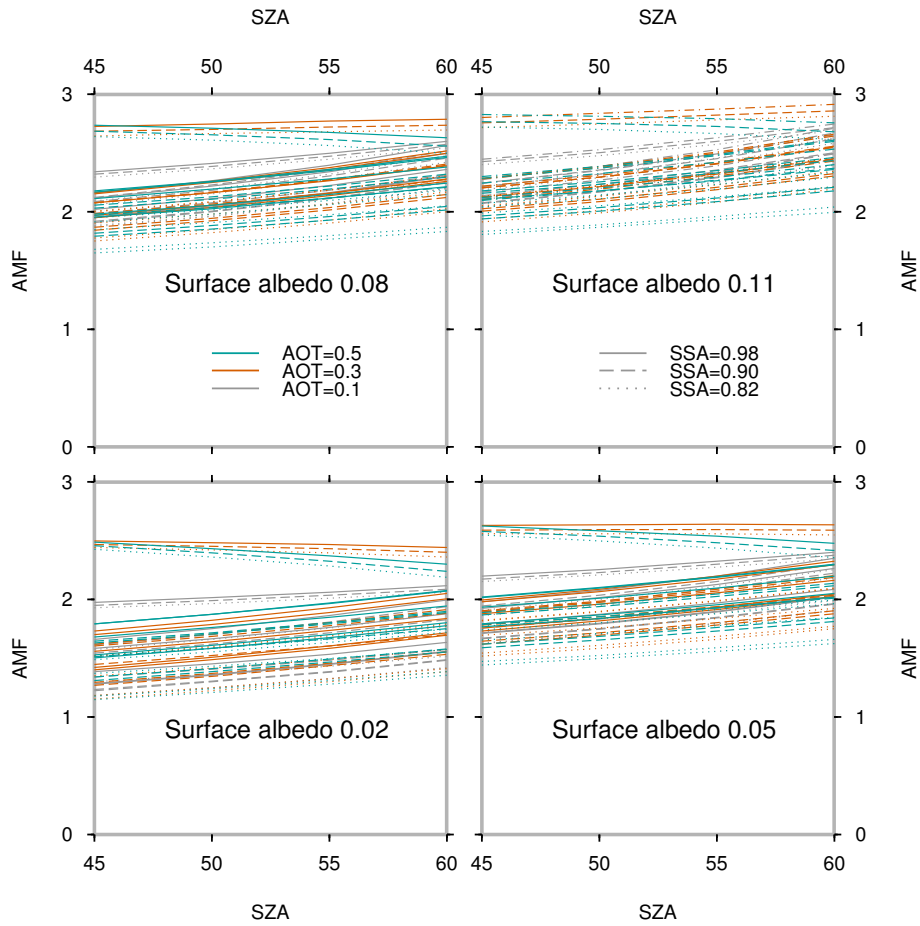


Figure 6. Calculated air-mass factors from the six high-surface-elevation (1400m) scenarios outlined in Fig. 4, plotted as a function of solar zenith angle and surface albedo. A dotted line indicates $\bar{\omega}=0.82$, a dashed line $\bar{\omega}=0.90$ and a solid line $\bar{\omega}=0.98$. AOT is indicated by line colour: grey for AOT=0.1, orange for AOT=0.3, and blue-green for AOT=0.5. At all surface albedos, the three upper curve families which stand out from the pack originate from Scenario 12.

the albedo map is limited to half a degree. Surface elevation is sampled from the US Geological Survey GTOPO-30 global digital elevation model with spatial resolution of ~~approximately~~ ~~approximately~~ 1km.

~~Aircraft SCDs are shifted using an offset to bring background aircraft VCD values in line with satellite tropospheric vertical column densities (TVCD), based on the assumption that the satellite instrument's background measurements over remote ocean areas better approximate a zero column measurement.~~ For the flight maps presented below, the mean of the minimum- and maximum ~~AMF was used to calculate the VCD~~; for the time-series plots the mean AMF is used ~~VCD is shown~~, with error-bars ~~defined by the~~ in the time-series plots defined by these ~~VCD's~~, calculated using the ~~minimum and maximum AMF~~ -maximum- and minimum AMF respectively. It should be noted that the mean does not represent the peak of the VCD probability density

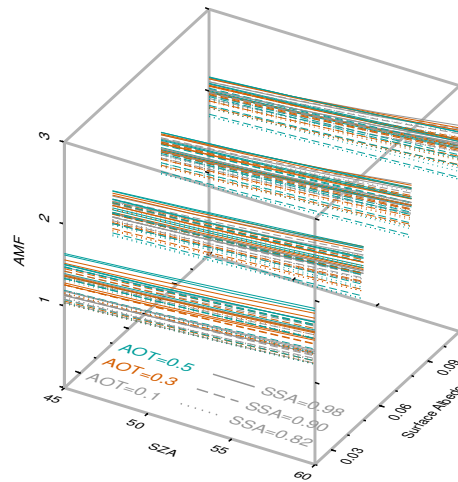


Figure 7. Calculated air-mass factors from the six low-surface-elevation scenarios outlined in Fig. 4, plotted as a function of solar zenith angle and surface albedo. A dotted line indicates $\bar{\omega}=0.82$, a dashed line $\bar{\omega}=0.90$ and a solid line $\bar{\omega}=0.98$. AOT is indicated by line colour: grey for AOT=0.1, orange for AOT=0.3, and blue-green for AOT=0.5. Variation in the AMF due to variations in aerosol properties and vertical profile shape are bounded by a minimum- and maximum-AMF surface at each surface elevation.

function as it might normally, and is used here as a shorthand to facilitate discussion. In reality there is only one correct vertical profile and associated AMF, so the true VCD is as likely to be the minimum or maximum as it is the mean.

In general cloud-free conditions were encountered during all of the flights. The exception to this is the flight on 11 August, where approximately one octa of thin cirrus cloud cover was observed above the aircraft, estimated to be at around 10000m.

- 5 Based on the radiative-transfer-modelling study of Kokhanovsky and Rozanov (2009), the TVCD error caused by clouds in the OMI measurement is estimated to be less than -10%. The effect of such clouds on errors in the aircraft measurement is not quantified, however it is likely to be less than this.

Flight on 9 August

- Figure 9 shows a map of tropospheric vertical column density (TVCD) from the Derivation of OMI tropospheric NO₂ (DOMINO) V2.0 product for 9 August 2007, with the flight track and NO₂ VCD from the airborne instrument overlaid.
- 10 The flight track is close to the eastern edge of the OMI pixel beneath it until approximately half-way between Johannesburg and Pretoria, where it crosses over to be on the western edge of the adjacent row of OMI pixels. Hourly-average wind directions from several weather stations are shown for the hour of the aircraft's overpass and the previous two hours. A time-series comparison of the airborne DOAS nadir NO₂ VCD with OMI TVCD on this day is shown in Fig. 10. In the time-series
- 15 plot, airborne DOAS measurements are shown with error-bars representing the uncertainty in the AMF, along with the OMI pixel at aircraft nadir (orange) as well as one OMI-row to the west (blue) and east (yellow) of the aircraft. ~~Spatially-averaged~~ Line-averaged full-resolution iDOAS measurements within the OMI pixel at aircraft nadir are shown in grey, with one standard deviation in measured variability above and below the average shown by error-bars. The first subsidiary plot in Fig. 10 shows

the surface elevation (grey) and surface albedo (orange) at aircraft nadir; the second subsidiary plot shows solar zenith angle at the aircraft's time and position (orange) as well as the minimum (grey) and maximum (cyan) AMF derived using the interpolation procedure described above. Aircraft time is indicated on the lower horizontal axis; the corresponding distance along the aircraft track is shown on the upper horizontal axis. Plots for subsequent flights present the measurements in a similar fashion.

5 Figure 11 shows the airborne full-resolution iDOAS measurements for all the flights, averaged within the satellite pixel at aircraft nadir, compared with the NO₂ TVCD satellite product in that pixel. Error bars once again indicate one standard deviation in measured variability above and below the average. The ~~figure inset shows a magnified view of the values lower than 7. The regression lines plotted in the inset regression lines~~ are fitted through value pairs with satellite TVCD ~~less greater~~ than 5 petamolec cm⁻²; ~~the regression lines in the main figure are fitted through value pairs with satellite TVCD greater than this.~~

10 The airborne iDOAS measurements on 9 August included background areas, industrial plumes and urban areas. Several cases are identified from the time-series shown in Fig. 10 and the map in Fig. 9, and shown in Table 2. Weather-station data from Grootvlei indicates an hourly-average wind direction of 219° and 3.1 m s⁻¹ for 12:00–13:00 UTC. The aircraft track is between 36 km–48 km downwind, and we might naively estimate that the plume is between approximately 3 h–4 h old when it was measured by the iDOAS.

Table 2. Cases of background, urban, and plume measurements identified from the iDOAS measurements on 9 August 2007. Aircraft time is given in UTC. OMI nadir refers ~~to the to the~~ TVCD value in the OMI pixel at aircraft nadir. Similarly, OMI east and OMI west refer to the OMI pixel one row east and west of aircraft nadir respectively. iDOAS peak refers to the peak VCD within the OMI pixel at aircraft nadir. iDOAS average is the ~~spatially averaged line-averaged~~ iDOAS measurements within the OMI pixel at aircraft nadir, and iDOAS standard deviation is the iDOAS-measured variability within this OMI pixel expressed as a standard deviation. iDOAS CV is the coefficient of variation (or relative standard deviation) of the measured variability. All column densities are expressed in petamolec cm⁻².

| Aircraft time | Description | OMI | | | iDOAS | | | | |
|---------------------|---------------------------|--------------------|--------------------|--------------------|--------------------------|------------------|---------------------|---------------------|---------------------|
| | | nadir | west | east | peak | avg. | std. dev. | CV | |
| 12:35 | 1.8 Background | 1.4 2.0 | 2.4 3.4 | 2.4 3.5 | 4.0 ± 0.4 | 1.1 | 1.8 0.97 | 1.1 0.94 | 0.61 0.9 |
| 12:45 | Plume | 11 | 34 | 7.8 | n/a | 11 10 | 4.6 4.4 | 0.41 0.4 | |
| 12:47 | Plume | 15 | 12 24 | 34 14 | 36 ± 5.5 | 12 | 29 27 | 3.7 3.6 | 0.13 0.1 |
| 12:50 51 | Peri-urban | 20 | 16 | 15 | n/a | 24 23 | 4.1 3.8 | 0.18 0.2 | |
| 12:53 | Urban industrial | 25 | 30 | 14 | 95 99 ± 15 | 23 | 60 56 | 22 21 | 0.36 0.4 |
| 12:55 | Urban industrial | 25 | 27 | 13 | n/a | 48 45 | 19 18 | 0.40 0.4 | |
| 12:59 | Urban | 16 | 7.6 | 3.7 | 11 14 ± 1.6 | 3.2 | 9.4 8.8 | 1.6 1.4 | 0.17 0.2 |
| 13:07 | Background | 0.8 | 1.3 | 2.0 | 2.1 4.9 ± 0.3 | 0.9 | 1.6 | 1.0 | 0.62 0.6 |

Examining the cases presented in Table 2, with reference to Figs. 9 and 10, where the data are presented on a map and as a time-series respectively, we find background measurements by the iDOAS and OMI at 12:35 and 13:07. In both cases the peak, and ~~spatially averaged iDOAS measurements are similar, with similar variability measured within each OMI pixel~~ ~~line-averaged~~

iDOAS VCD measurements are small. In the first case the OMI measurement is ~~the same magnitude as the~~ almost double the averaged iDOAS, in the second case it is half. The coefficient of variation (CV) of the background measurements is high, which indicates that the iDOAS is near its detection limit. At 12:45 and 12:55, horizontal gradients forming the shoulder of urban or ~~industial~~ industrial plumes are measured. At 12:45 the averaged iDOAS value closely matches the OMI measurement, however
5 this is by chance. The gradient across this OMI pixel is very steep, and the CV is high.

At 12:~~50~~ the 51 in the time-series the area between the two peaks ~~in the time-series~~ is measured. In this case the OMI and average iDOAS measurements are within 20% of each other, and the CV is relatively low. The two main peaks in the time-series are at 12:47 and 12:53. The former appears to be the plume originating from the Vaal Triangle, the latter is measured near O.R. Tambo International Airport in Johannesburg. The Vaal Triangle peak measured by the iDOAS is
10 ~~34~~36~~±5.5~~12 petamolec cm⁻², more than double the value of 15 measured by OMI. The ~~spatially-averaged~~ line-averaged iDOAS value is almost double the OMI measurement, and the peak serendipitously falls in the middle of the OMI pixel, so the CV is relatively low. Perhaps, since the aircraft is flying at the upwind edge of the nadir OMI pixel, the pixel to the west is a more appropriate comparison. In this case the iDOAS line-average is a better match.

The peak value near the airport measured by the iDOAS at 12:53 is ~~9599~~±1523 petamolec cm⁻². OMI fails to capture the
15 magnitude of this peak. Horizontal NO₂ gradients do not always conveniently align themselves with the flight directions of satellites and aircraft, and therefore a similar gradient in the orthogonal direction is likely, the west- and east OMI pixels also do not capture the peak. The imaging swath of the iDOAS is quite narrow, around 1980m, from 4500m above ground, which is too narrow to resolve the sort of gradient observed in the flight direction. A wider-swath imaging instrument may allow insights into the gradients within an OMI pixel. ~~Flying~~ In this case, flying the aircraft perpendicular to the satellite track rather
20 than along it might be ~~found to be~~ a better flight strategy to optimise the use of the imaging swath, since this will place the airborne instrument swath along the short axis of the satellite pixel. The ~~spatially-averaged~~ line-averaged OMI measurement of this peak is more than double the OMI value, with high variability within the pixel arising from the steep gradient.

In Fig. 11, ~~a regression line is fitted through OMI-pixel-averaged aircraft data compared with the OMI product, for values greater than 5. The slope of this~~ the slope of the regression line for this flight is ~~2.42~~2, indicating that for the ~~young~~ industrial
25 plumes and urban areas measured close to the sources during this flight, OMI substantially underestimates NO₂ VCD. This is likely to be because of poor horizontal dispersion of the plumes over the distance between the source and the measurement, however vertical dispersion may also play a role.

It is instructive to evaluate the potential air-mass factor error that might be made by assuming an incorrect vertical profile of NO₂. Several more radiative-transfer modelling scenarios are introduced, based on scenarios 11 and 12, i.e. with an exponentially-decreasing profile and surface elevation set at 1400m; some profiles with an elevated layer of NO₂ and some without. The scale height of the profiles is varied from 1400m to 200m, and radiative transfer calculations are done at a representative solar zenith angle of 55°. Once again air-mass factors for permutations of AOT of 0.1, 0.3, and 0.5, and SSA of 0.82, 0.90, and 0.98 are calculated. Results for aircraft- and satellite viewing geometry are presented in Fig. 8. The AMF increases for scenarios with an elevated NO₂ layer, the AMF increases as the vertical profile scale-height is decreased. In contrast, without such a layer, the AMF decreases as the scale-height is reduced. In the satellite viewing geometry, the behaviour
35

is slightly different compared to the aircraft geometry, with a flattening off of the AMFs with scale-heights of 600m and 400m in the elevated-layer scenarios. This behaviour can likely be explained by examination of the block-AMFs for the two cases, however such analysis is beyond the scope of the present study.

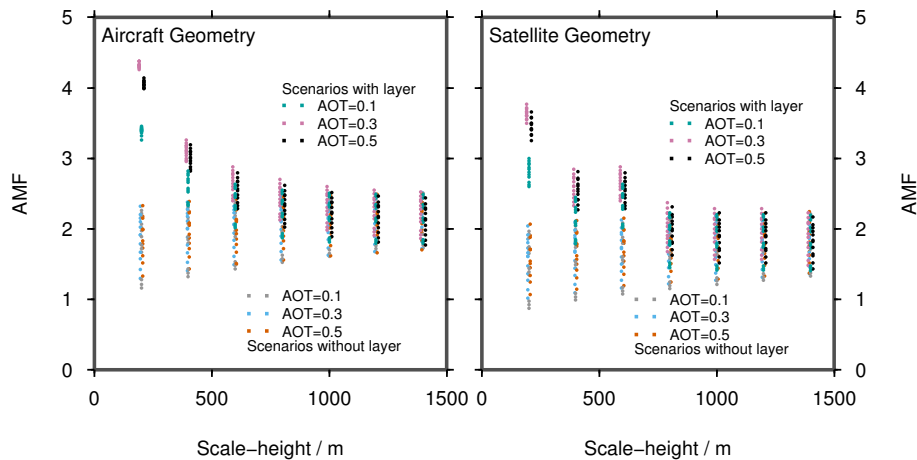


Figure 8. Air-mass factors at $SZA=55^\circ$ for scenarios based on an exponentially-decreasing vertical profile of NO_2 and aerosols, with scale heights varied from 1400m to 200m. These profiles are based on scenarios 11 and 12 from Fig. 4. Profiles with an elevated layer display an increasing trend of AMF with decreasing scale-height, those without the layer show a decrease in AMF.

We might estimate the VCD error arising from AMF uncertainty for the iDOAS using two profiles: the true profile at the spatial scale of the instrument, P_{true} and the profile used in the AMF calculation P_{prior} , along with the associated AMFs: AMF_{true} and AMF_{prior} . If P_{prior} is an exponentially-decreasing profile with scale-height of 1000m either with- or without an elevated layer, according to Fig 8 AMF_{prior} will lie between approximately 1.6 and 2.6. Close to a surface source of NO_2 P_{true} might have a much smaller scale-height, for example 400m. In the case of a profile with an elevated layer, AMF_{true} should be between 2.5 and 3.2. Using the mid-points of the uncertainty ranges of AMF_{true} and AMF_{prior} , this will lead to a 26% overestimation of the VCD. In the case of P_{true} having no elevated layer, AMF_{true} will lie between approximately 1.2 and 2.3, leading to a 20% underestimation of the VCD from the use of AMF_{prior} .

In the case of a satellite measurement, a representative profile for the satellite pixel is likely to have a larger scale-height, since more background areas will be included in the measurement along with the surface source, and the discrepancy between AMF_{prior} and AMF_{true} will be less, but will behave in a similar manner to that described above. This highlights the importance of an improved P_{prior} as the spatial resolution of the measurement improves. This has been implemented for OMI using a chemistry transport model at 0.667° by 0.5° resolution (compared to the global TM4 model's resolution of 3° by 2°) over eastern China, which resulted in an improved correlation with surface-based MAX-DOAS measurements (Lin et al., 2014). Future satellite missions which promise better spatial resolution (Veeffkind et al., 2012) will require improved prior vertical profile estimates in order to avoid this divergence in the VCD uncertainty over surface sources.

Table 3. Cases of background and plume measurements identified from the iDOAS measurements on 11 August 2007. Aircraft time is given in UTC. OMI nadir refers ~~to the~~ to the TVCD value in the OMI pixel at aircraft nadir. Similarly, OMI east and OMI west refer to the OMI pixel one row east and west of aircraft nadir respectively. iDOAS peak refers to the peak VCD within the OMI pixel at aircraft nadir. iDOAS average is the ~~spatially-averaged~~ line-averaged iDOAS measurements within the OMI pixel at aircraft nadir, and iDOAS standard deviation is the iDOAS-measured variability within this OMI pixel expressed as a standard deviation. iDOAS CV is the coefficient of variation (or relative standard deviation) of the measured variability. All column densities are expressed in petamolec cm⁻².

| Aircraft time | Description | OMI | | | iDOAS | | | |
|---------------|--------------------------------------|-------------------------|-------------------------|-------------------------|--|---------------------------|---------------------------|-----------------------------|
| | | nadir | west | east | peak | avg. | std. dev. | CV |
| 11:52 | <u>Background</u> | 2.4 | 3.1 | 4.0 | n/a | 2.4 <u>2.5</u> | 1.1 | 0.46 <u>0.44</u> |
| 12:14 | <u>Dispersed Plume</u> | 12 | 11 | 18 | 9.8 <u>14</u> ± 1.5 <u>3.0</u> | 8.9 <u>8.7</u> | 1.3 | 0.15 |
| 12:22 | 37 <u>Dispersed Plume</u> | 29 <u>31</u> | 21 | 36 | 43 <u>41</u> ± 7.0 <u>8.1</u> | 37 <u>32</u> | 3.9 <u>2.2</u> | 0.11 <u>0.06</u> |
| 12:25 | <u>Dispersed Plume</u> | 37 | 24 <u>30</u> | 29 <u>39</u> | 42 <u>44</u> ± 6.8 <u>9.4</u> | 36 | 2.4 <u>3.2</u> | 0.06 <u>0.09</u> |
| 12:32 | <u>Dispersed Plume</u> | 28 | 35 <u>36</u> | 16 <u>17</u> | 47 <u>48</u> ± 7.7 <u>11</u> | 44 <u>40</u> | 2.9 <u>3.1</u> | 0.07 <u>0.08</u> |

Flight on 11 August

On 11 August, the aircraft measured background values, as well as several cases of plumes originating from industrial facilities on the Highveld. Wind measurements at Camden of 8.6m s⁻¹ at 12:00 UTC allow a naïve estimate of the plume age from approximately 5h for the closest power station (approximately 145km as the wind blows) to 12h for the Vaal Triangle and the city of Johannesburg, approximately 360km away. In reality, the plumes are probably older than this, since the wind speeds in the 12h prior to the flight were lower, and this is confirmed by looking at a back-trajectory (not shown here) for air parcels over Swaziland for this day. This is slightly ~~older~~ further downwind than the Vaal Triangle plume measured on 9 August, and clearly much ~~older~~ further downwind than the NO₂ plume measured overhead the city of Johannesburg on that day, which is measured at the source.

10 These cases are enumerated in Table 3, which should be read in conjunction with Figs. 12 and 13. At 11:52, the iDOAS measured background NO₂ between Richards Bay and Swaziland. The ~~spatially-averaged~~ line-averaged iDOAS matches the satellite measurement. The measured variability is low, although the coefficient of variation (CV) is higher than for the other cases in Table 3. ~~This one~~ As is the case on 9 August, this again indicates that the iDOAS is operating close to its detection limit. The plume from the Vaal Triangle is measured at 12:14, in this case the OMI measurement is higher than ~~both the iDOAS~~ peak and spatial average values the iDOAS line-average value. The variability is similar to the background measurement, giving a much lower CV. At 12:22 and 12:25 the southern locus of a mega-plume appearing to originate from the Highveld is measured. In these cases, the ~~spatially-averaged~~ line-averaged iDOAS agrees well with the satellite measurement and the CV within each OMI pixel is very low. At 12:32 what appears to be the northern locus of the plume is measured by the iDOAS, with peak NO₂ VCD of ~~47~~ 48 ± ~~7.7~~ 11 petamolec cm⁻². This peak appears in the OMI measurement at a considerably lower magnitude,

although the upwind (west) pixel is more comparable with the iDOAS peak and average values. The coefficient of variation in this case is very low.

The reason for the dual locus of this plume is not clear; it is perhaps related to the topography where this plume appears to be on either side of a ridge. These two plume ~~loci~~ are resolved by the OMI satellite at aircraft nadir and one line upwind; one line downwind the two ~~loci~~ appear to have merged into one. The structure seen in the satellite image in Fig. 12 of a southern plume advecting from the Vaal Triangle, and a northern plume from Johannesburg and the cluster of power stations on the eastern Highveld is seen frequently while browsing through the OMI record. In Fig. 11 the regression line ~~in the main figure for this flight~~ has a slope of 1.1, indicating that OMI is better able to capture the shallower NO₂ VCD gradients in ~~an aged a dispersed~~ plume better than in the ~~young plumes narrow plumes near to emissions sources~~, and urban areas measured on 9 August.

Table 4. Cases of background and plume measurements identified from the iDOAS measurements on 18 August 2007. Aircraft time is given in UTC. OMI nadir refers ~~to the to the~~ TVCD value in the OMI pixel at aircraft nadir. Similarly, OMI east and OMI west refer to the OMI pixel one row east and west of aircraft nadir respectively. iDOAS peak refers to the peak VCD within the OMI pixel at aircraft nadir. iDOAS average is the ~~spatially averaged line averaged~~ iDOAS measurements within the OMI pixel at aircraft nadir, and iDOAS standard deviation is the iDOAS-measured variability within this OMI pixel expressed as a standard deviation. iDOAS CV is the coefficient of variation (or relative standard deviation) of the measured variability. All column densities are expressed in petamolec cm⁻².

| Aircraft time | Description | OMI | | | iDOAS | | | CV |
|---------------|--------------------------------------|---------------------------|--------------------------|-------------------------|--------------------------------------|-------------------------|---------------------------|-----------------------------|
| | | nadir | west | east | peak | avg. | std. dev. | |
| 12:41 | 15 <u>Dispersed plume</u> | 4.3 <u>8.2</u> | 11 <u>1.8</u> | 28 <u>10</u> | 22±5.1 <u>5.2</u> | 25 <u>23</u> | 2.1 <u>1.9</u> | 0.08 |
| 12:45 | 22 <u>Plume</u> | 24 <u>29</u> | 18 <u>32</u> | 58 <u>23</u> | 61±11 <u>15</u> | 47 <u>43</u> | 7.3 <u>6.9</u> | 0.16 |
| 12:54 | <u>Plume</u> | 39 | 35 | 32 | 64 <u>67±11</u> <u>16</u> | 58 <u>53</u> | 5.8 <u>5.2</u> | 0.10 |
| 13:01 | <u>Plume</u> | 40 | 30 | 24 | 82 <u>84±14</u> <u>21</u> | 68 <u>63</u> | 12 <u>11</u> | 0.18 <u>0.17</u> |
| 13:03 | <u>Plume</u> | 44 | 43 | 34 | 63 <u>79±11</u> <u>20</u> | 57 <u>53</u> | 7.8 <u>7.2</u> | 0.14 |

Flight on 18 August

The flight on 18 August, shown in Fig. 14, routed close to the power stations on the Eastern Highveld. Several plumes are identified from the iDOAS measurement time-series in Fig. 15 and the map in Fig. 14 and summarised in Table 4. The aircraft track was approximately 55km downwind of Majuba, 110km downwind of Tutuka power station and 140km downwind of Secunda. The Vaal Triangle was approximately 250km upwind of the aircraft. Weather station measurements from Tutuka indicate windspeeds of 2.1 m s⁻¹, giving a naïve estimate of plume age ranging from 7h from Majuba to 18h from Secunda. All of the cases in Table 4 are plume measurements. In all the cases both the peak and the ~~spatially averaged line averaged~~ iDOAS measurements are higher than the OMI measurement. The coefficients of variation are generally intermediate between those found on 9 and 11 August.

The regression through OMI-pixel-averaged aircraft measurements compared with the OMI product from 18 August in Fig. 11 has a slope of $\underline{+51.3}$. This reflects the lower NO_2 VCDs measured by OMI in comparison to the iDOAS, described above in relation to the time-series in Fig. 15.

Comparing the three flights that were performed to track the Aura satellite, we find a relation between the slope of the regression line and the distance of the measurement from the source. For the flight on 9 August, which passed approximately 40km downwind of the Vaal Triangle and directly overhead Johannesburg the slope of the regression line is $\underline{2.42.2}$. Measurements on 11 August, between 145 – 360km downwind of sources give a slope of 1.1 and the measurements on 18 August, where the aircraft was 55 – 150km downwind of major sources gives an intermediate slope of $\underline{+51.3}$. There appears to be a similar relation between distance downwind and coefficient of variation within each OMI pixel. This is what we would expect, since a more dispersed plume would have lower horizontal gradients, and hence a better match between the satellite and iDOAS. Plume dispersion occurs by turbulent mixing in the boundary layer, which is related to surface topography and instability (i.e. thermals). Both of these are spatial features of the landscape hence the relationship of degree of mixing with distance downwind, rather than the time taken to travel the distance. An additional effect evident from the modelling results in Fig. 8 is that AMF errors will be less when there is more vertical dispersion, and therefore a profile with a higher scale-height.

Comparison studies of ground-based multi-axis DOAS (MAX-DOAS) instruments with satellite measurements have given mixed results. Some studies (Irie et al., 2008; Hains et al., 2010) show MAX-DOAS results consistently lower than OMI. Kanaya et al. (2009) show DOMINOv2 biases of up to 50% lower than the MAX-DOAS, although the bias improves when only remote surface sites are considered. This is attributed to both horizontal inhomogeneity within the OMI pixels and the inability of OMI to observe NO_2 close to the surface.

It is clear from inspection of the peak iDOAS measurements in Tables 2, 3, and 4 that our approach of using a range of AMFs to calculate the VCD results in a variability in the VCD that scales with SCD. This is simply a mathematical effect that is obvious from Eq. 2. It is interesting to note in the OMI measurements that the downwind pixels (yellow in the time-series plots) reproduce the plume structures observed in the aircraft-nadir OMI pixels (bold orange), with in general lower VCD. This would indicate a steady decrease in the amount of NO_2 in the air, probably due to chemical conversion into another species.

Flight on 14 August

A comparison between the airborne iDOAS and SCIAMACHY can be made from the flight on 14 August. Several cases identified in Fig. 16 and 17 are summarised in Table 5. The background measurements at 08:17 and 08:27 by SCIAMACHY and iDOAS are similar, and once again the coefficient of variation (CV) is high. Plumes are measured at 07:56, 08:01, and 08:08. In each case, the average iDOAS is lower than the SCIAMACHY measurement, although the CV is higher than for other flights. At 08:12 the iDOAS measured the gradient on the shoulder of a plume, in this case the average iDOAS and the SCIAMACHY measurement are close, and the CV is similar to the gradient measurement at 12:55 on 9 August (shown in Table 2)

Examining Fig. 11 we see that the slope of the regression line between SCIAMACHY and the averaged iDOAS is less than unity, indicating that the iDOAS underestimates relative to SCIAMACHY. Comparing the performance of OMI and

SCIAMACHY against the iDOAS, one would expect OMI, given its higher spatial resolution, to be better able to capture the peak VCD's in the narrow plumes found on the Highveld. ~~It appears that this is not the case, however the reason for this is not clear; perhaps it is related to the different instantaneous fields of view of the two instruments.~~ Given that we have only one SCIAMACHY comparison, it is difficult to draw any firm conclusion here.

Table 5. Cases of background and plume measurements identified from the iDOAS measurements on 14 August 2007. Aircraft time is given in UTC. SCIA nadir refers ~~to the~~ to the TVCD value in the SCIAMACHY pixel at aircraft nadir. iDOAS peak refers to the peak VCD within the OMI pixel at aircraft nadir. iDOAS average is the ~~spatially-averaged line-averaged~~ iDOAS measurements within the SCIAMACHY pixel at aircraft nadir, and iDOAS standard deviation is the iDOAS-measured variability within this SCIAMACHY pixel expressed as a standard deviation. iDOAS CV is the coefficient of variation (or relative standard deviation) of the measured variability. All column densities are expressed in petamolec cm^{-2} .

| Aircraft time | Description | SCIA nadir | iDOAS peak | iDOAS avg | iDOAS std deviation | iDOAS CV |
|---------------|--------------------------------------|------------|--|---------------------------|---------------------------|-----------------------------|
| 07:56 | 19 <u>Dispersed plume</u> | 19 | 21 <u>21 ± 3.3</u> 2.7 | 13 <u>12</u> | 4.9 <u>4.6</u> | 0.37 <u>0.38</u> |
| 08:01 | <u>Plume</u> | 19 | 32 <u>32.34 ± 5.4</u> 8.9 | 16 <u>14</u> | 9.1 <u>8.4</u> | 0.56 <u>0.60</u> |
| 08:08 | <u>Plume</u> | 10 | 21 <u>21.23 ± 3.6</u> 5.6 | 9.4 <u>9.0</u> | 5.9 <u>5.5</u> | 0.63 <u>0.61</u> |
| 08:12 | <u>Plume / background</u> | 7.6 | 5.9 <u>12 ± 1.0</u> 2.9 | 5.3 <u>4.8</u> | 2.4 <u>2.2</u> | 0.45 <u>0.46</u> |
| 08:17 | <u>Background</u> | 6.3 | 4.2 <u>7.8 ± 0.6</u> 1.9 | 3 <u>2.8</u> | 1.6 <u>1.5</u> | 0.53 |
| 08:27 | <u>Background</u> | 4.1 | 4.2 <u>8.7 ± 0.6</u> 2.0 | 3.4 | 1.8 <u>1.5</u> | 0.53 <u>0.44</u> |

5 6 Conclusions

Four research flights were performed over the Highveld region of South Africa during August 2007 using an airborne imaging DOAS instrument to measure NO_2 column densities, a Particle Measurement Systems PCASP probe to measure aerosol size distribution and number density, and a chemiluminescence in-situ NO_y instrument. These flights were planned to co-incide with overpasses of the OMI and SCIAMACHY satellite instruments, with the aircraft measurements within an hour of the satellite. Each flight included a vertical profile measurement at the beginning and end of the airborne DOAS measurement segment.

Vertical profile measurements of NO_y and aerosol particle number concentrations, although compromised by problems with instruments and limitations due to flight safety requirements, reveal several features consistent with profiles reported in the literature. Profile shapes can be approximated by a block-shape and an exponentially-decreasing profile of trace-gas and aerosol concentration, and elevated layers of enhanced concentration are ~~frequently~~ sometimes present over the Highveld. Observations of aerosol optical thickness and single-scattering albedo from AERONET during July to September 2007 and 2009 are used to determine representative values for these parameters.

These observations are used to devise a number of scenarios, which are used in a sensitivity study using the SCIATRAN radiative transfer model. A minimum- and maximum air-mass factor is found for a given combination of surface elevation

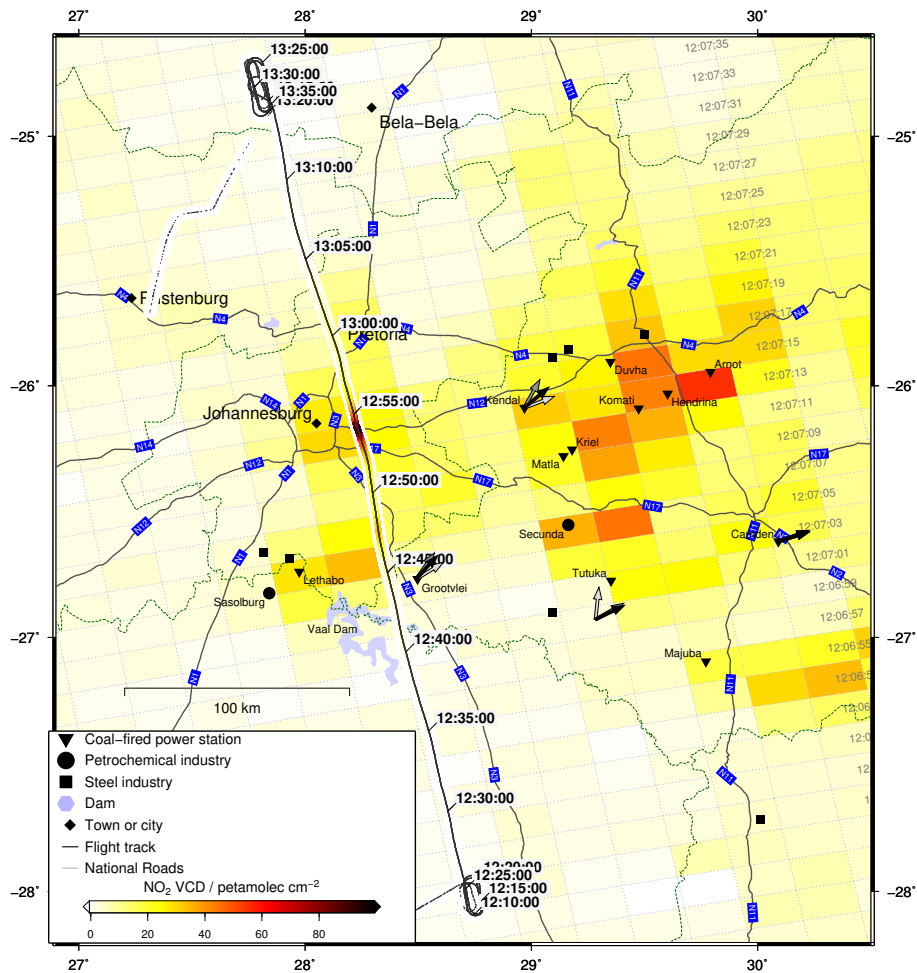


Figure 9. A comparison of the [10-second moving average](#) airborne DOAS NO_2 vertical column densities (indicated by colour along the flight track) with OMI DOMINO V2.0 (coloured rectangles) on 9 August 2007. UTC aircraft time is indicated every five minutes along the flight track (black line running from approximately 28°S , 28.8°E to 24.8°S , 27.8°E). UTC satellite time is shown for each row. Hourly-average wind directions for several weather stations are shown for the hours up to 13:00 UTC (black arrow), 12:00 UTC (dark grey arrow) and 11:00 UTC (light grey arrow).

and albedo, and solar zenith angle. The difference between the minimum and maximum air-mass factor represents uncertainty due to the profile shape and aerosol properties. These air-mass factor estimates are used to calculate vertical column densities from the slant-column densities measured by the iDOAS instrument. These are then compared to satellite tropospheric NO_2 products from OMI and SCIAMACHY.

- 5 The present approach to quantification of the uncertainty in the air-mass factor, and hence vertical column density, implies that the uncertainty in the vertical column density scales with the magnitude of the slant column density, in cases where the uncertainty in the air-mass factor is the dominant source of error.

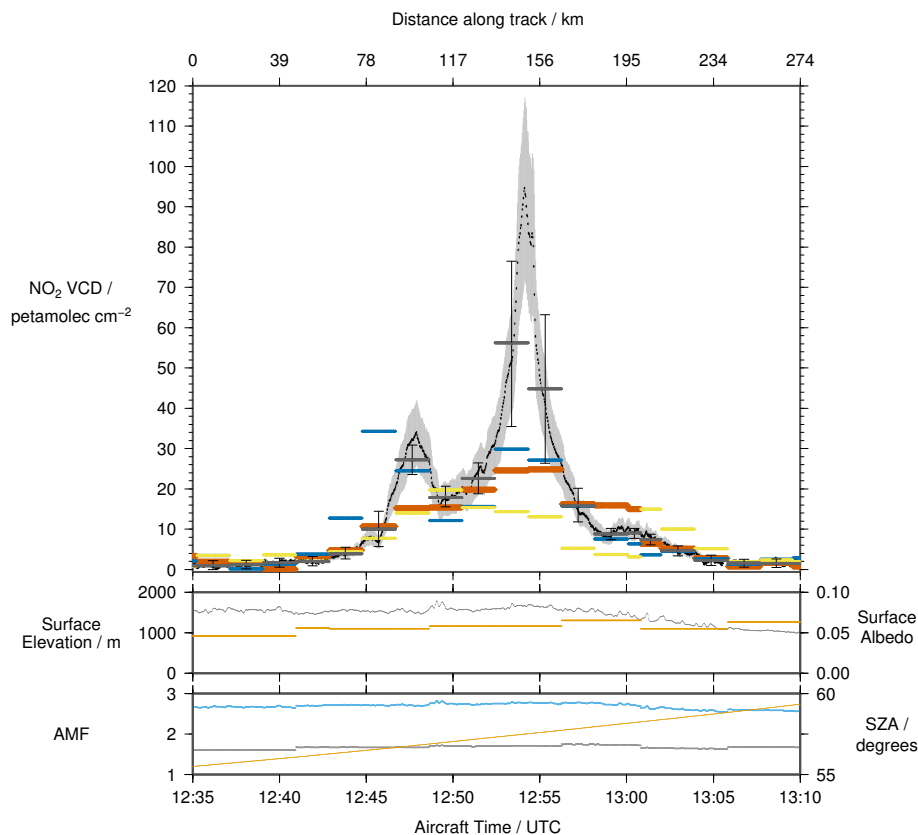


Figure 10. A timeseries of the airborne DOAS NO₂ vertical column densities on 9 August 2007, DOMINO V2.0 at aircraft nadir (orange) and one OMI line west (blue) and east (yellow) of aircraft nadir. Aircraft measurements averaged over the [area-length](#) of each OMI pixel are shown in grey, with one standard deviation in measured variability above and below the average indicated with error-bars. Surface elevation ([grey](#)) and surface albedo ([orange](#)) are shown in the first sub-plot. The second sub-plot shows the minimum and maximum AMF estimates (grey and blue), and the solar zenith angle (orange) at aircraft time and position.

[Analysis of air-mass factors from vertical profiles with a variety of scale-heights indicates that uncertainty increases as the scale-height decreases, as may be the case when making high spatial resolution measurements close to a surface source of NO₂. Indeed, the presence or absence of an elevated layer, leads to uncertainty in the sign of the error in the air-mass factor. This implies that air-mass factor errors will be less further downwind of sources, where vertical mixing within the boundary layer has taken place.](#)

The airborne DOAS instrument's much higher spatial resolution, even when averaged using a moving average on a spatial scale of approximately 1.2km, reveals spatial gradients in NO₂ that are much steeper than those observed by the satellites. Large-scale features are resolved by the satellites, however peak NO₂ vertical column densities observed by the aircraft close to urban and industrial sources are in some cases more than twice the satellite measurement. The performance of the satellite measurement was found to better for more dispersed plumes, measured further downwind from the source.

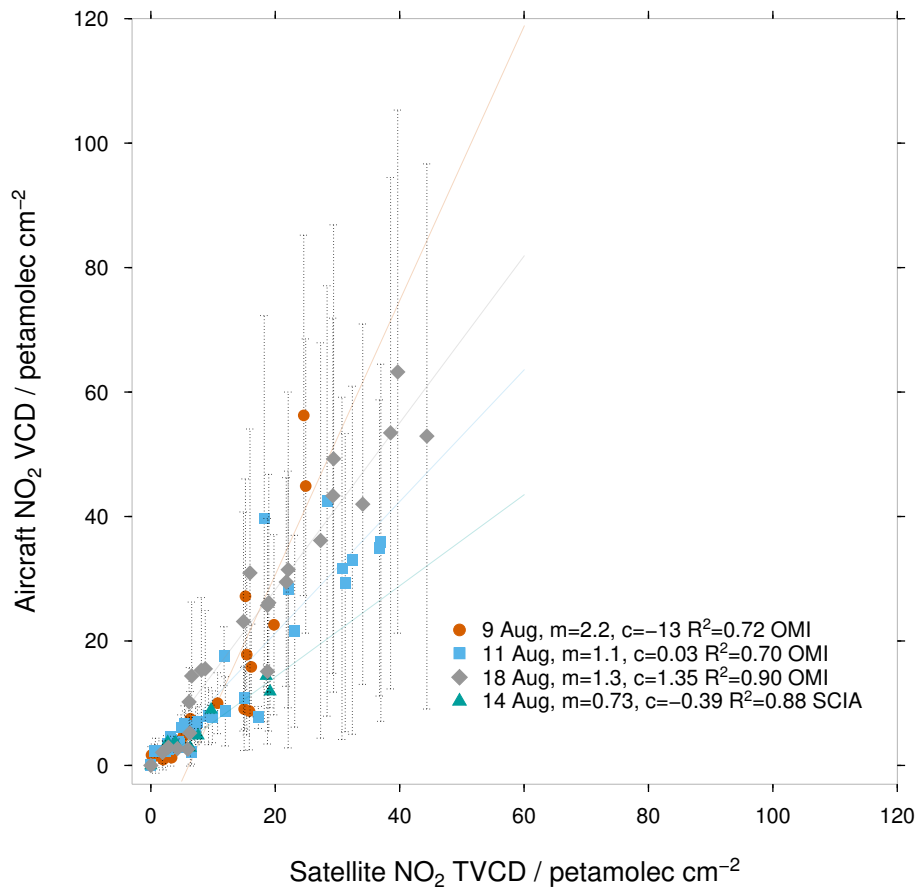


Figure 11. OMI and SCIAMACHY measurements compared with co-located spatially-averaged line-averaged aircraft measurements. Aircraft iDOAS VCD is calculated using the mean of the minimum- and maximum-AMF calculated for the high-resolution measurement. Error-bars indicate the minimum- and maximum iDOAS VCD found within the satellite pixel. In the inset figure, a linear regression line is fitted through all background measurements less than 5 petamolec cm^{-2} . In the main figure, the regression lines are fitted through measurements greater than 5 petamolec cm^{-2} for each flight. The slope (m) of the regression line for each day is indicated, as well as the y-intercept (c) and the regression coefficient (R^2).

For measurements further than approximately 150km downwind, the agreement between the aircraft and OMI is within the margin of error of approximately ~~30~~40% arising from uncertainty in the air-mass factor. This is due to the decrease in horizontal NO_2 gradients from turbulence in the mixed layer, which is dependent on spatial features such as surface topography and the characteristics of thermals during the day. As such the agreement between the spatially-averaged iDOAS NO_2 VCD and the satellite product improves with distance, better than it does with time, downwind of the source.

Inspection of OMI Level-2 satellite images allow plumes from certain point sources on the Highveld to be identified. In other cases, plumes from areas containing several point sources, or effective area sources such as the city of Johannesburg can be identified. During the winter, these plumes are sufficiently stable that they retain their structure for several hundred kilometers

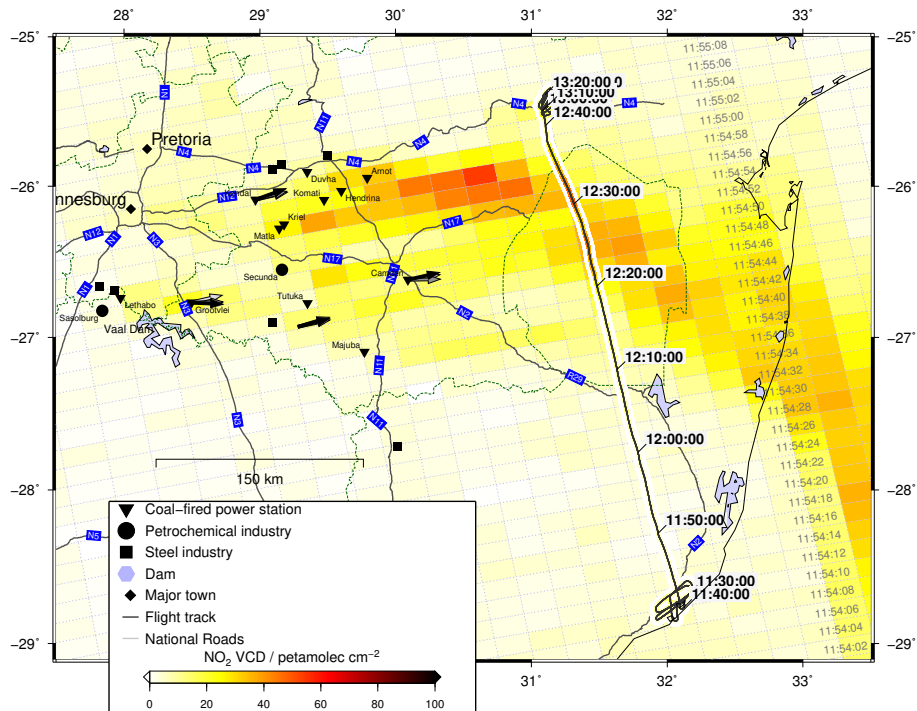


Figure 12. A comparison of the airborne DOAS 10-second moving average NO_2 vertical column densities between Richards Bay and Nelspruit with OMI DOMINO V2.0 on 11 August 2007. Data presentation is as in Fig. 9.

downwind. This leads to a northern- and southern plume being visible on the satellite image, corresponding to sources on the eastern Highveld and the Vaal Triangle.

The high spatial resolution of the airborne instrument reveals spatial features in the NO_2 distribution that are not visible even at the relatively high resolution of the OMI sensor. Upcoming satellite missions such as TROPOMI (Veefkind et al., 2012), which have a higher spatial resolution than OMI promise to reveal small-scale features using daily measurements from space, however improved prior vertical profiles will be needed to constrain the air-mass factor uncertainty close to surface sources.

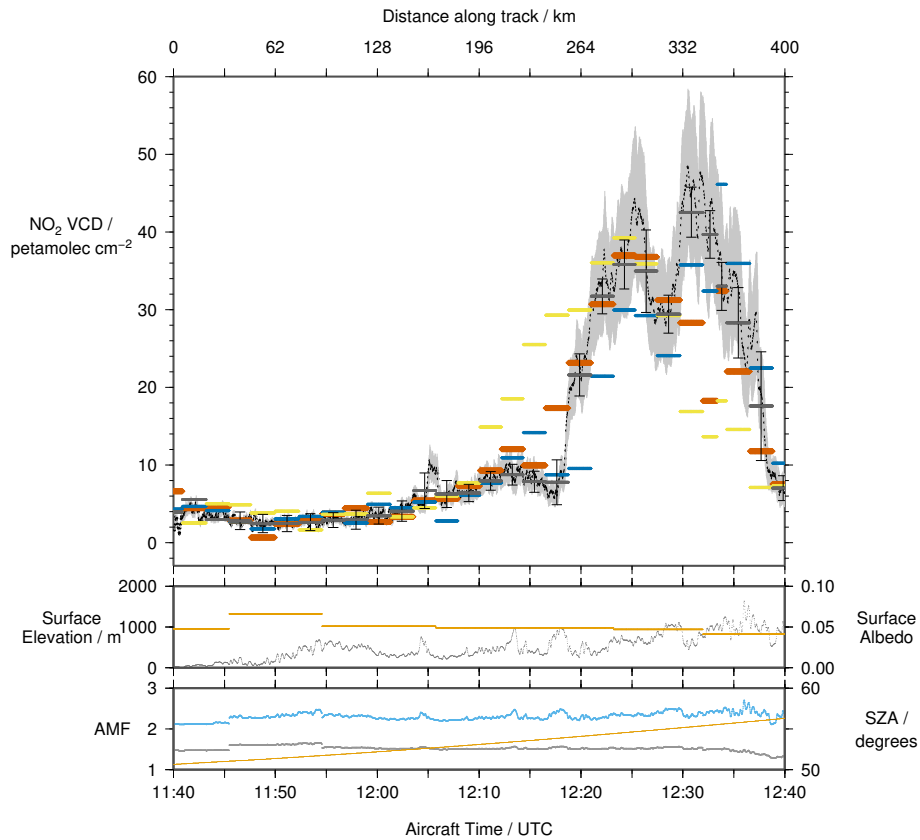


Figure 13. A timeseries of the airborne DOAS NO_2 vertical column densities on 11 August 2007, DOMINO V2.0 at aircraft nadir (orange) and one OMI line west (blue) and east (yellow). Aircraft measurements averaged over the area-length of each OMI pixel are shown in grey. Sub-plots are as described for Fig. 10.

Acknowledgements. GTOPO-30 DEM data is available from the U.S. Geological Survey. Funding was received from Eskom SOC Ltd. for this project. Thanks to the South African Weather Service, and aircraft crews for support during field campaigns. We acknowledge the free use of tropospheric NO_2 column data from the OMI sensor from www.temis.nl. Alexander Kokhanovsky acknowledges support of the excellence centre from applied mathematics and theoretical physics within MEPhI Academic Excellence Project (contract No.

5 02.a03.21.0005,27.08.2013)

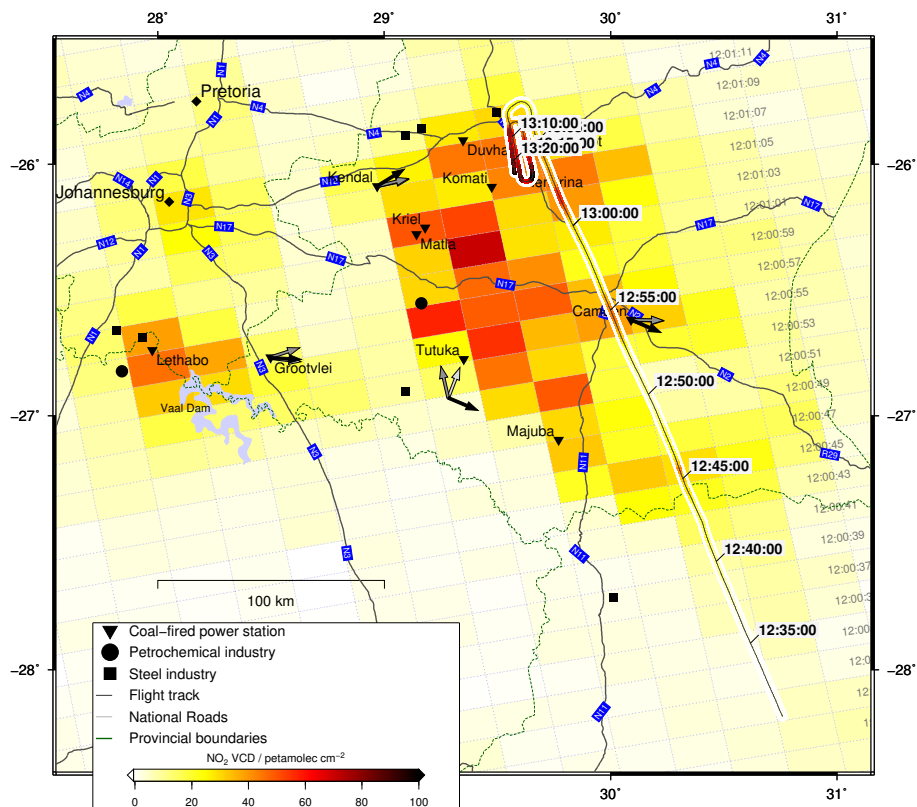


Figure 14. A comparison of the airborne DOAS [10-second moving average](#) NO₂ vertical column densities with DOMINO V2.0 on 18 August 2007. Data presentation is as in Fig. 9

References

- Annegarn, H. J., Otter, L., Swap, R. J., and Scholes, R. J.: Southern African's ecosystem in a test-tube, *South African Journal of Science*, 98, 111–113, 2002.
- Balashov, N. V., Thompson, A. M., Piketh, S. J., and Langerman, K. E.: Surface ozone variability and trends over the South African Highveld from 1990 to 2007, *Journal of Geophysical Research: Atmospheres*, pp. 4323–4342, doi:10.1002/2013JD020555. Received, 2014.
- 5 Beirle, S., Boersma, K. F., Platt, U., Lawrence, M. G., and Wagner, T.: Megacity emissions and lifetimes of nitrogen oxides probed from space., *Science (New York, N.Y.)*, 333, 1737–9, doi:10.1126/science.1207824, <http://www.ncbi.nlm.nih.gov/pubmed/21940891>, 2011.
- Boersma, K. F., Eskes, H. J., Dirksen, R. J., van der A, R. J., Veeckind, J. P., Stammes, P., Huijnen, V., Kleipool, Q. L., Sneep, M., Claas, J., Leitão, J., Richter, A., Zhou, Y., and Brunner, D.: An improved tropospheric NO₂ column retrieval algorithm for the Ozone Monitoring Instrument, *Atmospheric Measurement Techniques*, 4, 1905–1928, doi:10.5194/amt-4-1905-2011, <http://www.atmos-meas-tech.net/4/1905/2011/>, 2011.
- 10 Burrows, J., Richter, A., Dehn, a., Deters, B., Himmelmann, S., Voigt, S., and Orphal, J.: Atmospheric Remote-Sensing Reference Data From Gome—2. Temperature-Dependent Absorption Cross Sections of O₃ in the 231–794Nm Range, *Journal of Quantitative Spectroscopy and*

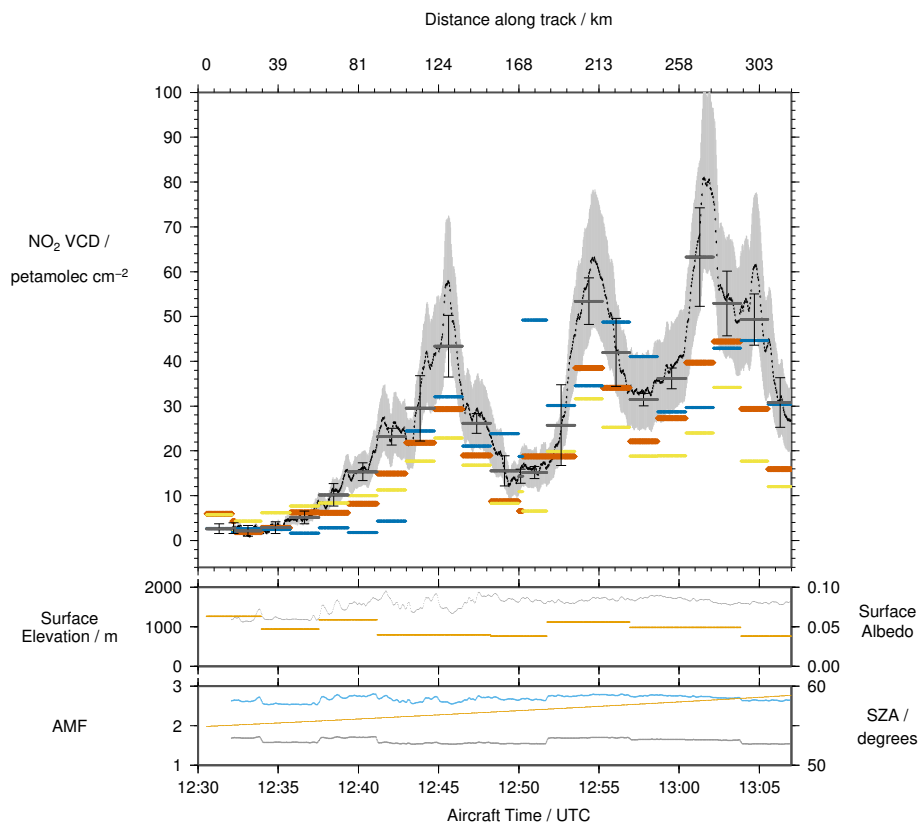


Figure 15. A timeseries of the airborne DOAS NO₂ vertical column densities on 18 August 2007, DOMINO V2.0 at aircraft nadir (orange) and one OMI line west (blue) and east (yellow). Aircraft measurements averaged over the [area-length](#) of each OMI pixel are shown in grey. Sub-plots are as described for Fig. 10

Radiative Transfer, 61, 509–517, doi:10.1016/S0022-4073(98)00037-5, <http://linkinghub.elsevier.com/retrieve/pii/S0022407398000375>, 1999.

Collett, K. S., Piketh, S. J., and Ross, K. E.: An assessment of the atmospheric nitrogen budget on the South African Highveld, South African Journal of Science, 106, 1–9, doi:10.4102/sajs.v106i5/6.220, <http://www.sajs.co.za/index.php/SAJS/article/view/220>, 2010.

- 5 Dentener, F. J., van Weele, M., Krol, M., Houweling, S., and van Velthoven, P.: Trends and inter-annual variability of methane emissions derived from 1979-1993 global CTM simulations, Atmospheric Chemistry and Physics, 3, 73–88, doi:10.5194/acpd-2-249-2002, 2003.
- Eck, T. F.: Variability of biomass burning aerosol optical characteristics in southern Africa during the SAFARI 2000 dry season campaign and a comparison of single scattering albedo estimates from radiometric measurements, Journal of Geophysical Research, 108, doi:10.1029/2002JD002321, <http://www.agu.org/pubs/crossref/2003/2002JD002321.shtml>, 2003.
- 10 Gottwald, M., Bovensmann, H., and (Eds): SCIAMACHY, Exploring the Changing Earth's Atmosphere, Springer Dordrecht Heidelberg London New York, doi:10.1007/978-90-481-9896-2, 2006.
- Greenblatt, G., Orlando, J., Burkholder, J., and Ravishankara, A. R.: Absorption measurements of Oxygen between 330nm and 1140nm, Journal of Geophysical Research, 95, 18 577–18 582, 1990.

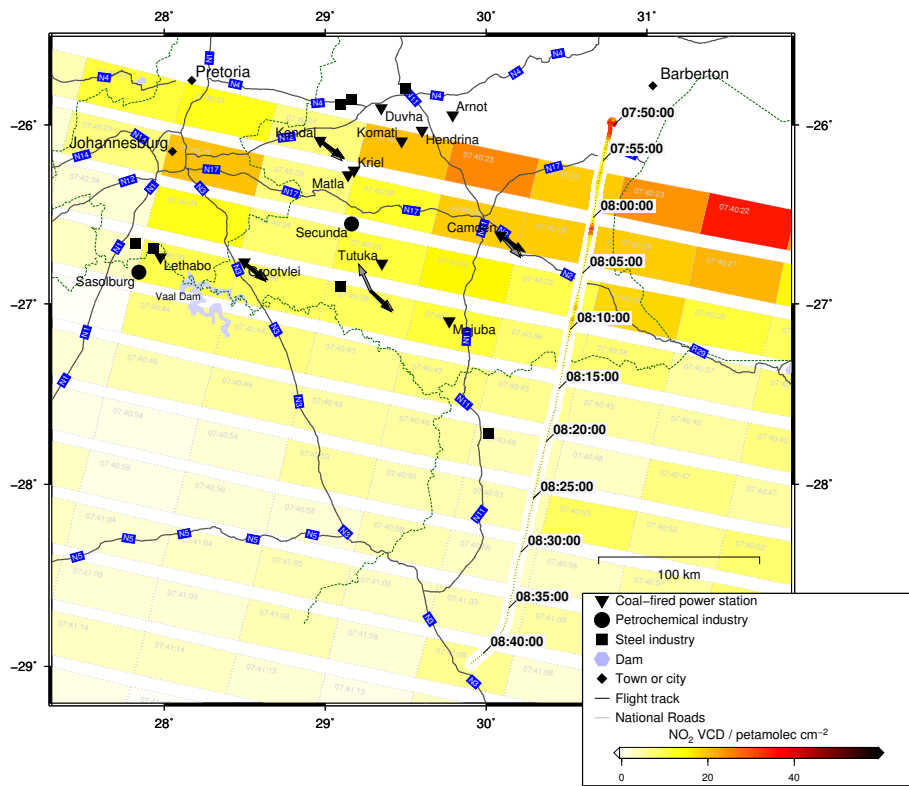


Figure 16. A comparison of the airborne DOAS 10-second moving average NO_2 vertical column densities with SCIAMACHY on 14 August 2007. Data presentation is as in Fig. 9, however since SCIAMACHY is a whiskbroom instrument, times-the-time for each satellite pixel are is shown in each pixel. SCIAMACHY overpass was at around 07:40 UTC.

- Hains, J. C., Boersma, K. F., Kroon, M., Dirksen, R. J., Cohen, R. C., Perring, A. E., Bucsela, E., Volten, H., Swart, D. P. J., Richter, A., Wittrock, F., Schoenhardt, A., Wagner, T., Ibrahim, O. W., van Roozendaal, M., Pinardi, G., Gleason, J. F., Veefkind, J. P., and Levelt, P. F.: Testing and improving OMI DOMINO tropospheric NO_2 using observations from the DANDELIONS and INTEX-B validation campaigns, *Journal of Geophysical Research*, 115, 1–20, doi:10.1029/2009JD012399, 5 <http://www.agu.org/pubs/crossref/2010/2009JD012399.shtml>, 2010.
- Haywood, J. M.: Comparison of aerosol size distributions, radiative properties, and optical depths determined by aircraft observations and Sun photometers during SAFARI 2000, *Journal of Geophysical Research*, 108, doi:10.1029/2002JD002250, <http://www.agu.org/pubs/crossref/2003/2002JD002250.shtml>, 2003a.
- Haywood, J. M.: The mean physical and optical properties of regional haze dominated by biomass burning aerosol measured from the C-130 aircraft during SAFARI 2000, *Journal of Geophysical Research*, 108, doi:10.1029/2002JD002226, 10 <http://www.agu.org/pubs/crossref/2003/2002JD002226.shtml>, 2003b.
- Heney, L. and Greenstein, J.: Diffuse radiation in the galaxy, *Astrophysical Journal*, 93, 70–83, doi:10.1086/144246, 1941.

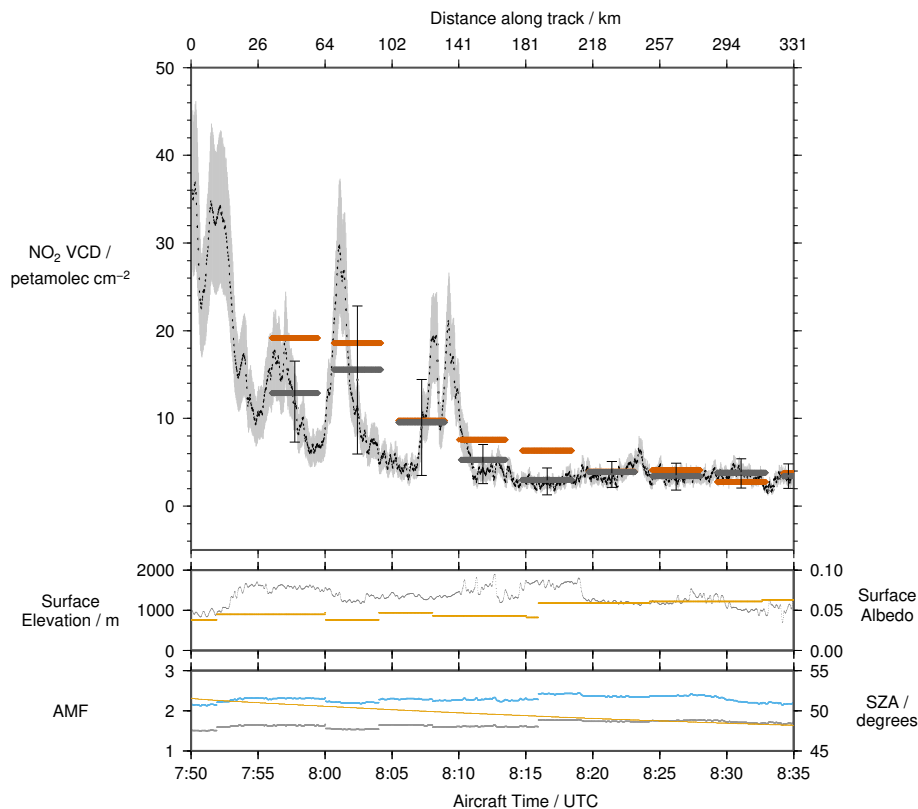


Figure 17. A timeseries of the airborne DOAS NO_2 vertical column densities on 14 August 2007, and SCIAMACHY at aircraft nadir (orange) and OMI DOMINO V2.0 at aircraft nadir (yellow). Aircraft measurements averaged over the area-length of each OMI-SCIAMACHY pixel are shown in grey. Sub-plots are as described for Fig. 10

- Heue, K.-P., Wagner, T., Broccardo, S. P., Walter, D., Piketh, S. J., Ross, K. E., Beirle, S., and Platt, U.: Direct observation of two dimensional trace gas distributions with an airborne Imaging DOAS instrument, *Atmospheric Chemistry and Physics*, 8, 6707–6717, doi:10.5194/acp-8-6707-2008, <http://www.atmos-chem-phys.net/8/6707/2008/>, 2008.
- Hobbs, P. V.: Clean air slots amid dense atmospheric pollution in southern Africa, *Journal of Geophysical Research*, 108, 1–8, doi:10.1029/2002JD002156, <http://www.agu.org/pubs/crossref/2003/2002JD002156.shtml>, 2003.
- Holben, B. N., Tanre, D., Smirnov, A., Eck, T. F., Slutsker, I., Abuhassan, N., Newcomb, W. W., Schafer, J. S., Chatenet, B., Lavenu, F., Kaufman, Y. J., Castle, J. V., Setzer, A., Markham, B., Clark, D., Frouin, R., Halthore, R., Karneli, A., O'Neill, N. T., Pietras, C., Pinker, R. T., Voss, K., and Zibordi, G.: An emerging ground-based aerosol climatology : Aerosol optical depth from AERONET, *Journal of Geophysical Research*, 106, 12 067–12 097, 2001.
- 10 Irie, H., Kanaya, Y., Akimoto, H., Tanimoto, H., Wang, Z., Gleason, J. F., and Bucsela, E. J.: Validation of OMI tropospheric NO_2 column data using MAX-DOAS measurements deep inside the North China Plain in June 2006 : Mount Tai Experiment 2006, *Atmospheric Chemistry and Physics*, pp. 6577–6586, 2008.
- Kanaya, Y., Irie, H., Takashima, H., Iwabuchi, H., Akimoto, H., Sudo, K., Gu, M., Chong, J., and Kim, Y. J.: Long-term MAX-DOAS network observations of NO_2 in Russia and Asia (MADRAS) during the period 2007 – 2012 : instrumentation, elucidation of climatology ,

- and comparisons with OMI satellite observations and global model simulations, *Atmospheric Chemistry and Physics*, pp. 7909–7927, doi:10.5194/acp-14-7909-2014, 2014.
- Kleipool, Q. L., Dobber, M. R., de Haan, J. F., and Levelt, P. F.: Earth surface reflectance climatology from 3 years of OMI data, *Journal of Geophysical Research: Atmospheres*, 113, 1–22, doi:10.1029/2008JD010290, 2008.
- 5 Kokhanovsky, A. A. and Rozanov, V. V.: Retrieval of NO₂ vertical columns under cloudy conditions : A sensitivity study based on SCIATRAN calculations, *Atmospheric Research*, 93, 695–699, doi:10.1016/j.atmosres.2009.01.022, <http://dx.doi.org/10.1016/j.atmosres.2009.01.022>, 2009.
- Kraus, S. G.: DOASIS: A Framework Design for DOAS, Ph.D. thesis, Mannheim, 2006.
- Laakso, L., Vakkari, V., Virkkula, a., Laakso, H., Backman, J., Kulmala, M., Beukes, J. P., van Zyl, P. G., Tiitta, P., Josipovic, M., Pienaar, J. J., Chiloeane, K., Gilardoni, S., Vignati, E., Wiedensohler, a., Tuch, T., Birmili, W., Piketh, S. J., Collett, K., Fourie, G. D., Komppula, M., Lihavainen, H., de Leeuw, G., and Kerminen, V.-M.: South African EUCAARI measurements: seasonal variation of trace gases and aerosol optical properties, *Atmospheric Chemistry and Physics*, 12, 1847–1864, doi:10.5194/acp-12-1847-2012, <http://www.atmos-chem-phys.net/12/1847/2012/>, 2012.
- 10 Leitão, J., Richter, A., Vrekoussis, M., Kokhanovsky, A., Zhang, Q. J., Beekmann, M., and Burrows, J.: On the improvement of NO₂ satellite retrievals – aerosol impact on the airmass factors, *Atmospheric Measurement Techniques*, 3, 475–493, doi:10.5194/amt-3-475-2010, 2010.
- Levelt, P. F., Oord, G. H. J. V. D., Dobber, M. R., Mälkki, A., Visser, H., Vries, J. D., Stammes, P., Lundell, J. O. V., and Saari, H.: The Ozone Monitoring Instrument, *IEEE Transactions on Geoscience and Remote Sensing*, 44, 1093–1101, 2006.
- Lin, J.-T., Martin, R. V., Boersma, K. F., Sneep, M., Stammes, P., Spurr, R., Wang, P., Van Roozendaal, M., Clémer, K., and Irie, H.: Retrieving tropospheric nitrogen dioxide from the Ozone Monitoring Instrument: effects of aerosols, surface reflectance anisotropy, and vertical profile of nitrogen dioxide, *Atmospheric Chemistry and Physics*, 14, 1441–1461, doi:10.5194/acp-14-1441-2014, <http://www.atmos-chem-phys.net/14/1441/2014/>, 2014.
- 20 Liu, Y. and Daum, P. H.: THE EFFECT OF REFRACTIVE INDEX ON SIZE DISTRIBUTIONS AND LIGHT SCATTERING COEFFICIENTS DERIVED FROM OPTICAL PARTICLE COUNTERS, *Journal of Aerosol Science*, 31, 945–957, 2000.
- Lourens, A., Butler, T., Beukes, J. P., van Zyl, P. G., Beirle, S., Wagner, T., Heue, K.-P., Pienaar, J. J., Fourie, G. D., and Lawrence, M. G.: Re-evaluating the NO₂ hotspot over the South African Highveld, *South African Journal of Science*, 108, 1–6, 2012.
- 25 Maenhaut, W., Salma, I., and Cafrneyer, J.: Regional atmospheric aerosol composition and sources in the eastern Transvaal, South Africa, and impact of biomass burning, *Journal of Geophysical Research*, 101, 23 613–23 650, 1996.
- Magi, B. I., Hobbs, P. V., Schmid, B., and Redemann, J.: Vertical profiles of light scattering, light absorption, and single scattering albedo during the dry, biomass burning season in southern Africa and comparisons of in situ and remote sensing measurements of aerosol optical depths, *Journal of Geophysical Research*, 108, doi:10.1029/2002JD002361, <http://www.agu.org/pubs/crossref/2003/2002JD002361.shtml>, 2003.
- 30 Martin, R. V., Chance, K. V., Jacob, D. J., Kurosu, T. P., Spurr, R. J. D., Bucsela, E. J., Gleason, J. F., Palmer, P. I., Bey, I., Fiore, A. M., Li, Q., Yantosca, R. M., and Koelemeijer, R. B.: An improved retrieval of tropospheric nitrogen dioxide from GOME, *Journal of Geophysical Research*, 107, doi:10.1029/2001JD001027, <http://www.agu.org/pubs/crossref/2002/2001JD001027.shtml>, 2002.
- 35 McLinden, C. a., Fioletov, V., Boersma, K. F., Krotkov, N. A., Sioris, C. E., Veeffkind, J. P., and Yang, K.: Air quality over the Canadian oil sands: A first assessment using satellite observations, *Geophysical Research Letters*, 39, n/a–n/a, doi:10.1029/2011GL050273, <http://doi.wiley.com/10.1029/2011GL050273>, 2012.

- Mclinden, C. A., Fioletov, V., Shephard, M. W., Krotkov, N., Li, C., Martin, R. V., Moran, M. D., and Joiner, J.: Space-based detection of missing sulfur dioxide sources of global air pollution, *Nature Geoscience*, pp. 1–7, doi:10.1038/NNGEO2724, 2016.
- Platt, U. and Stutz, J.: *Differential Optical Absorption Spectroscopy*, Springer-Verlag, Berlin, Heidelberg, 1st edn., 2008.
- Rhodes, B.: pyEphem Home Page, <http://rhodesmill.org/pyephem/>, 2015.
- 5 Richter, A., Burrows, J. P., Nüss, H., Granier, C., and Niemeier, U.: Increase in tropospheric nitrogen dioxide over China observed from space., *Nature*, 437, 129–32, doi:10.1038/nature04092, <http://www.ncbi.nlm.nih.gov/pubmed/16136141>, 2005.
- Rosenberg, P. D., Dean, A. R., Williams, P. I., Dorsey, J. R., Minikin, A., Pickering, M. A., and Petzold, A.: Particle sizing calibration with refractive index correction for light scattering optical particle counters and impacts upon PCASP and CDP data collected during the Fennec campaign, *Atmospheric Measurement Techniques*, 5, 1147–1163, doi:10.5194/amt-5-1147-2012, 2012.
- 10 Rothman, L., Rinsland, C., Goldman, a., Massie, S., Edwards, D., Flaud, J.-M., Perrin, a., Camy-Peyret, C., Dana, V., Mandin, J.-Y., Schroeder, J., Mccann, a., Gamache, R., Wattson, R., Yoshino, K., Chance, K., Jucks, K., Brown, L., Nemtchinov, V., and Varanasi, P.: the Hitran Molecular Spectroscopic Database and Hawks (Hitran Atmospheric Workstation): 1996 Edition, *Journal of Quantitative Spectroscopy and Radiative Transfer*, 60, 665–710, doi:10.1016/S0022-4073(98)00078-8, <http://linkinghub.elsevier.com/retrieve/pii/S0022407398000788>, 1998.
- 15 Rozanov, V. V. and Rozanov, A. V.: Differential optical absorption spectroscopy (DOAS) and air mass factor concept for a multiply scattering vertically inhomogeneous medium: theoretical consideration, *Atmospheric Measurement Techniques*, 3, 751–780, doi:10.5194/amt-3-751-2010, <http://www.atmos-meas-tech.net/3/751/2010/>, 2010.
- Rozanov, V. V., Rozanov, A. V., Kokhanovsky, A. A., and Burrows, J. P.: Radiative transfer through terrestrial atmosphere and ocean: Software package SCIATRAN, *Journal of Quantitative Spectroscopy and Radiative Transfer*, 133, 13–71, doi:10.1016/j.jqsrt.2013.07.004, 20
<http://dx.doi.org/10.1016/j.jqsrt.2013.07.004>, 2014.
- Stein, A. F., Draxler, R. R., Rolph, G. D., Stunder, B. J. B., Cohen, M. D., and Ngan, F.: NOAA’s hysplit atmospheric transport and dispersion modeling system, *Bulletin of the American Meteorological Society*, 96, 2059–2077, doi:10.1175/BAMS-D-14-00110.1, 2015.
- Streets, D. G., Canty, T., Carmichael, G. R., Foy, B. D., Dickerson, R. R., Duncan, B. N., Edwards, D. P., Haynes, J. A., Henze, D. K., Houyoux, M. R., Jacob, D. J., Krotkov, N. A., Lamsal, L. N., Liu, Y., Lu, Z., Martin, R. V., Gabriele, G. P., Pinder, R. W., Salawitch,
25 R. J., and Wecht, K. J.: Emissions estimation from satellite retrievals : A review of current capability, *Atmospheric Environment*, 77, 1011–1042, doi:10.1016/j.atmosenv.2013.05.051, 2013.
- Swap, R. J. and Tyson, P. D.: Stable discontinuities as determinants of the vertical distribution of aerosols and trace gases in the atmosphere, *South African Journal of Science*, 95, 63–71, 1999.
- Toenges-Schuller, N., Stein, O., Rohrer, F., Wahner, a., Richter, A., Burrows, J. P., Beirle, S., Wagner, T., Platt, U.,
30 and Elvidge, C. D.: Global distribution pattern of anthropogenic nitrogen oxide emissions: Correlation analysis of satellite measurements and model calculations, *Journal of Geophysical Research*, 111, D05 312, doi:10.1029/2005JD006068, <http://doi.wiley.com/10.1029/2005JD006068><http://www.agu.org/pubs/crossref/2006/2005JD006068.shtml>, 2006.
- van der A, R. J., Eskes, H. J., Boersma, K. F., Noije, T. P. C. V., Roozendaal, M. V., De Smedt, I., Peters, D. H. M. U., Meijer, E. W., van Noije, T. P. C., Van Roozendaal, M., De Smedt, I., Peters, D. H. M. U., and Meijer, E. W.: Trends, seasonal variability and dominant NO_x source
35 derived from a ten year record of NO₂ measured from space, *Journal of Geophysical Research*, 113, 1–12, doi:10.1029/2007JD009021, <http://www.agu.org/pubs/crossref/2008/2007JD009021.shtml>, 2008.

Vandaele, A. C., Hermans, C., Simon, P. C., Carleer, M., Colin, R., Fally, S., Merienne, M. F., Jenouvrier, A., and Coquart, B.: MEASUREMENTS OF THE NO₂ ABSORPTION CROSS-SECTION FROM 42 000 cm⁻¹ TO 10 000 cm⁻¹ (238-1000 nm) AT 220 K AND 294 K, *Journal of Quantitative Spectroscopy and Radiative Transfer*, 59, 171–184, 1998.

5 Veefkind, J. P., Aben, I., McMullan, K., Förster, H., de Vries, J., Otter, G., Claas, J., Eskes, H., de Haan, J., Kleipool, Q., van Weele, M., Hasekamp, O., Hoogeveen, R., Landgraf, J., Snel, R., Tol, P., Ingmann, P., Voors, R., Kruizinga, B., Vink, R., Visser, H., and Levelt, P. F.: TROPOMI on the ESA Sentinel-5 Precursor: A GMES mission for global observations of the atmospheric composition for climate, air quality and ozone layer applications, *Remote Sensing of Environment*, 120, 70–83, doi:10.1016/j.rse.2011.09.027, <http://linkinghub.elsevier.com/retrieve/pii/S0034425712000661>, 2012.